Neural correlates and determinants of approach-avoidance conflict in the prelimbic prefrontal cortex

Fernandez-Leon, J.A.[#1,2]; Engelke, D.S.[#1]; Aquino-Miranda, G.[#1]; Goodson, A.[3]; Do-Monte, F.H.[1,3]*.

[1] Dept. of Neurobiology & Anatomy, The University of Texas Health Science Center, Houston, TX77030, USA;

[2] Current Address: Exact Sciences Faculty, INTIA (UNCPBA-CICPBA) and CIFICEN (UNCPBA-CONICET-CICPBA), Tandil 7000, Buenos Aires, Argentina;

[3] Rice University, Houston, TX77030, USA

[#] These authors contributed equally to this work

*Corresponding author:

Fabricio H. Do Monte, DVM, PhD.
Department of Neurobiology and Anatomy, McGovern Medical School,
The University of Texas Health Science Center at Houston
6431 Fannin Street, Room 7.166, Houston, Texas 77030
Phone: 713-500-5613
Email: fabricio.h.domonte@uth.tmc.edu

Keywords: Prelimbic prefrontal cortex, electrophysiology, optogenetics, fear, reward, decision-making.

ABSTRACT

The recollection of environmental cues associated with threat or reward allows animals to select the most appropriate behavioral responses. Neurons in the prelimbic cortex (PL) respond to both threat- and reward-associated cues. However, it remains unknown whether PL regulates threat-avoidance vs. reward-approaching responses when an animals' decision depends on previously associated memories. Using a conflict model in which rats retrieve memories of shock- and food-paired cues, we observed two distinct phenotypes during conflict: i) rats that continued to press a lever for food (*Pressers*); and ii) rats that exhibited a complete suppression in food seeking (*Non-Pressers*). Single-unit recordings revealed that increased risk-taking behavior in *Pressers* is associated with persistent food-cue responses in PL, and reduced spontaneous activity in PL glutamatergic (PL^{GLUT}) neurons during conflict. Activating PL^{GLUT} neurons in *Pressers* attenuated food-seeking responses in a neutral context, whereas inhibiting PL^{GLUT} neurons in *Non-Pressers* reduced defensive responses and increased food approaching during conflict. Our results establish a causal role for PL^{GLUT} neurons in mediating individual variability in memory-based risky decision making by regulating threat-avoidance vs. reward-approach behaviors.

INTRODUCTION

The brain's ability to identify and discriminate cues associated with threat or reward allows organisms to respond appropriately to changes in the environment (Schultz, 2015; Hu, 2016). Animals respond to threatening cues with a series of defensive behaviors including avoidance responses that decrease their chances of being exposed to aversive outcomes (McNaughton and Corr, 2014; Krypotos et al., 2015; Cain, 2019). In contrast, reward cues have attractive and motivational properties that elicit approach behavior (Robinson and Flagel, 2009; Morales and Berridge, 2020). When animals are exposed to threat and reward cues simultaneously, an approach-avoidance conflict emerges, and decision-making processes are recruited to resolve the situation (Kirlic et al., 2017; Barker et al., 2019). While many studies have investigated the neural mechanisms that control threat-avoidance and reward-approach independently of each other, it is unclear how the brain uses previously learned information to regulate the opposing behavioral drives of avoiding threats and seeking rewards during a conflict situation.

Neurons in the prelimbic (PL) subregion of the medial prefrontal cortex (mPFC) change their firing rates in response to cues that predict either threat or reward (Baeg et al., 2001; Burgos-Robles et al., 2009; Burgos-Robles et al., 2013; Moorman and Aston-Jones, 2015; Dejean et al., 2016; Otis et al., 2017). Accordingly, activity in PL neurons is necessary for the retrieval of both food- and threat-associated memories (Sierra-Mercado et al., 2011; Courtin et al., 2014; Sangha et al., 2014; Do-Monte et al., 2015; Otis et al., 2017). PL neurons are reciprocally connected with the basolateral nucleus of the amygdala (BLA) (McDonald, 1991; Vertes, 2004), a region implicated in the

92 detection of threats or rewards (Amir et al., 2015; Namburi et al., 2015; Beyeler et al.,
93 2016; Zhang et al., 2020). During a risky foraging task in rats, dynamic modifications in
94 the activity of PL and BLA neurons correlate with the detection of imminent threats and
95 the defensive readiness for action (Kim et al., 2018; Kyriazi et al., 2020). In addition,
96 during a modified Pavlovian cue discrimination task involving footshocks as punishment,
97 increased activity in the BLA-PL pathway is sufficient and necessary for the expression
98 of freezing responses (Burgos-Robles et al., 2017), , a passive form of defensive
99 behavior. Conversely, inhibitory signaling in PL neurons correlates with threat
100 avoidance (Diehl et al., 2018), an active form of defensive behavior. While these studies
101 suggest a potential role of PL during motivational conflict involving states of certainty
102 (i.e., imminent threats), it is unknown whether changes in PL activity underlie the
103 behavioral variability in approach-avoidance responses under states of uncertainty,
104 when decision depends entirely on the retrieval of associated memories. It is also
105 unclear whether PL activity is necessary to coordinate appropriate behavioral responses
106 during conflict, and if so, which sub-types of PL neurons govern the competing
107 demands of approaching rewards vs. avoiding potential threats.

108 To address these questions, we designed an approach-avoidance conflict test
109 that assess the ability of rats to remember cues previously associated with either food
110 or footshocks to make a behavioral decision. Using a combination of optogenetics and
111 single-unit recordings, we investigated rats' individual variability in reward seeking and
112 defensive responses during the conflict test and correlated their behaviors (e.g.
113 freezing, avoidance, risk-assessment) with the firing rate of photoidentified
114 glutamatergic and GABAergic neurons in PL. We then examined the role of PL neurons

in risky decision-making by optogenetically manipulating PL activity with high temporal resolution and cell-type specificity during the conflict test.

RESULTS

Rats show individual variability in reward-seeking and defensive responses during the approach-avoidance conflict test.

To investigate the motivational conflict between approaching rewards and avoiding potential threats, we established a behavioral model in which rats need to balance food seeking with conditioned defensive responses based on their memories of previously acquired cues. Food-restricted rats (18 g of chow per day) were initially placed in an operant box and trained to press a lever for sucrose in the presence of audiovisual cues that signaled the availability of food. Each lever press during the audiovisual cue presentation resulted in the delivery of a sucrose pellet into a nearby dish (see Methods for details). When rats reached 50% of discrimination during cued food-seeking, they began lever-pressing for sucrose preferentially during the audiovisual cues (**Supplementary Fig. 1A-B**). During the habituation day, rats were placed in an odor arena and familiarized with the food cues and the neutral odor amyl acetate (see Methods for details). Next, to pair the odor cue with an aversive stimulus, rats were exposed to an olfactory threat conditioning training (Day 1). Animals were placed in an operant box (conditioning box; **Fig. 1A left**) previously connected to an olfactometer and habituated to one odor presentation (amyl acetate, 30 s) without footshock, followed by five odor presentations of the same odor that co-terminated with an

electrical footshock (0.7 mA, 1 s duration, 270-390 s inter-trial intervals, **Fig. 1A far-left**). Food cues (30 s duration) were presented during the inter-trail intervals to assess lever press suppression. Rats showed robust defensive responses during the threat conditioning training, as evidenced by an increase in freezing during the conditioned odor presentation (**Fig. 1B**), a decrease in lever presses (**Fig. 1C**), and an increase in the latency to press the lever (**Fig. 1D**) during the presentation of the food cues across trials. After rats have acquired the reward and threat associations, they were returned to the same odor arena in which they were previously habituated and exposed to a test session (Day 2) (**Fig 1A, right**). The test session consisted of three different phases: (i) a *Reward Phase*, in which only the audiovisual cues signaling the availability of food were presented; (ii) an *Odor Phase*, in which only the conditioned odor was presented, and a (iii) *Conflict phase*, in which both the food cues and the conditioned odor were presented simultaneously (**Fig 1A, far-right**).

During the reward phase, rats spent ~40% of the time in the food area and pressed the lever for food in ~95% of the food cue trials, without exhibiting significant defensive behaviors (**Fig. 1E-J**). Introduction of the shock-paired odor during the odor phase reduced the percentage of time rats spent in the food area to ~15%, and increased defensive behaviors characterized by heightened freezing, avoidance, and risk-assessment responses (**Fig. 1E-H**). These defensive behaviors were attenuated by the introduction of food cues during the conflict phase, as evidenced by a reduction in the percentage of time avoiding the threatening odor **(Fig. 1F)** and an increase in the percentage of time approaching the food area **(Fig. 1H)**. This indicates that the concomitant presentation of food cues and shock-paired odor induced a behavioral

conflict in the animals. Interestingly, when we analyzed the percentage of rewarded presses during the conflict phase **(Fig. 1J)**, two behavioral phenotypes emerged: *i)* rats that continued to press the lever for food in the presence of the threatening odor (*Pressers,* **Fig. 1K**); and *ii)* rats that showed a complete suppression in lever presses in the presence of the threatening odor (*Non-Pressers*, **Fig. 1L**). We then separated the animals into two different groups and compared their behaviors during the entire test session **(Fig. 1K-R, Supplementary Movie 1)**. While *Pressers* and *Non-Pressers* showed similar behavioral responses during the reward phase (all p values > 0.05), *Pressers* showed a lower percentage of time exhibiting freezing and avoidance responses **(Fig. 1M,N)**, and a greater percentage of time approaching the food area **(Fig. 1P)** when compared to *Non-Pressers* during both the odor and the conflict phases. These individual phenotypes were not due to prior behavioral differences between the two groups because *Pressers* and *Non-Pressers* showed similar lever pressing rates during the cued food-seeking training, as well as the same levels of freezing, velocity (i.e., maximum speed), and lever presses during the threat conditioning phase (**Supplementary Fig. 1A-E**), indicating that increased risk-taking behavior in *Pressers* was not caused by prior differences in reward-seeking motivation. Together, our results demonstrate that our conflict model is a suitable paradigm to investigate the interactions between reward- and threat-associated memories. Given that rats exhibit individual differences in food seeking and defensive responses during the test session, we next took advantage of the two observed phenotypes to examine the neuronal correlates of risk-taking (*Pressers*) and risk-avoiding (*Non-Pressers*) behaviors in PL neurons.

PL neurons respond differently to reward cues in *Pressers* vs. *Non-Pressers* during conflict.

To investigate the role of PL neurons in regulating food-approach and threat-avoidance responses, we performed single-unit recordings across the different phases of the conflict test **(Fig. 2A)**. We aligned the activity of PL neurons to the onset of the food cues during the reward phase and tracked the firing rates of the same cells during the conflict phase. Using the behavioral classification shown in **Fig. 1J**, we separated the animals into *Pressers* or *Non-pressers* and compared changes in PL activity in response to food cues during the reward and conflict phases **(Fig. 2B-V)**. When PL activity was time-locked to the onset of the food cues during the reward phase, *Pressers* showed a higher number of food-cue responsive neurons than *Non-Pressers* **(Fig. 2C-D vs. Fig. 2M-N)**, with the proportion of excitatory and inhibitory responses being similar between the two groups. During the conflict phase, both *Pressers* and *Non-Pressers* showed a significant reduction in the number of food-cue responsive neurons (**Fig. 2C-D vs. 2M-N**), suggesting that PL neurons can distinguish between reward and conflict situations. However, *Pressers* exhibited persistent excitatory food cue responses **(Fig. 2E vs. Fig. 2O)**, which were higher in magnitude than in *Non-Pressers* **(Fig. 2F vs. Fig. 2P).** In addition, *Pressers* showed a higher magnitude of inhibitory food-cue responses during the reward phase and, in contrast to *Non-Pressers*, such responses were attenuated during the conflict phase **(Fig. 2FI-J vs. Fig. 2S-T).**

Next, we time-locked the activity of PL neurons to the onset of the food cues during the conflict phase. We observed a larger number of food-cue responsive neurons in *Pressers* compared to *Non-Pressers* **(Supplementary Fig. 2A-B vs. Supplementary**

Fig. 2K-L). Moreover, *Pressers* showed a higher magnitude of excitatory food cue responses during the conflict phase compared to *Non-Pressers* **(Supplementary Fig. 2C-F vs. Supplementary Fig. 2M-P)**, while the magnitude of the inhibitory food cue responses in *Pressers* were higher during the conflict phase compared to the reward phase **(Supplementary Fig. 2G-J vs. Supplementary Fig. 2Q-T)**.

To further explore whether changes in activity dynamics of PL neurons differ between *Pressers* and *Non-Pressers*, we compared the spontaneous firing rate of the neurons before vs. after each phase of the test session **(Supplementary Fig. 3A)**. While *Pressers* showed the same proportion of excitation and inhibition across the different phases, *Non-Pressers* exhibited a significant increase in the proportion of excitation during the conflict phase **(Supplementary Fig. 3B)**. This suggests that increased spontaneous activity in PL neurons during the conflict phase may be associated with the complete suppression in lever presses observed in *Non-Pressers* **(Fig. 1J)**. Collectively, these results suggest that differences in the number and magnitude of excitatory food cue responses, as well as in the spontaneous activity of PL neurons, during the conflict phase may contribute to the individual differences in risky decision-making observed between the two behavioral phenotypes.

Different subsets of PL neurons signal freezing, avoidance, and risk-assessment behaviors in both *Pressers* and *Non-pressers*.

To investigate whether PL activity correlates with the expression of distinct defensive behaviors during the test session, we used a pose estimation algorithm (Deep Lab Cut, see Methods for details) to identify the onset of freezing, avoidance or risk-assessment

responses and align these time points with the activity of PL neurons. We found that a small percentage of PL neurons changed their firing rates during the onset of freezing (**Fig. 3A**), avoidance (**Fig. 3B**), or risk-assessment (**Fig. 3C**) behaviors in both *Pressers* and *Non-Pressers*, with a similar proportion of excitatory and inhibitory responses being observed in the two groups **(Fig. 3A-I)**. Interestingly, most PL responsive neurons (80%) changed their activities exclusively during the onset of one of these three behaviors, with avoidance-responsive cells also responding during the onset of risk-assessment behavior **(Fig. 3J-M)**. These results suggest that different subsets of PL neurons signal distinct behavioral outcomes during a conflict situation, with only a reduced number of PL neurons encoding the aversive salience of environmental cues independently of the behavioral defensive response expressed by the animal.

***Pressers* and *Non-Pressers* show significant differences in delta and theta oscillations in PL**

Previous studies have shown that oscillations in mPFC neuronal activity at different frequency bands correlate with distinct behavioral states in both rodents and humans (Narayanan et al., 2013; Harris and Gordon, 2015). Neural oscillations in the mPFC emerge from the network of excitatory and inhibitory synaptic connections and are thought to contribute to neural communication when subjects engage in reward and threat memory tasks (Hyman et al., 2011; Likhtik and Paz, 2015; Park and Moghaddam, 2017; Widge et al., 2019). To investigate whether *Pressers* and *Non-Pressers* show significant differences in PL oscillations during conflict, we recorded local field potentials (LFPs) from PL neurons and calculated the average of power spectral density (PSD) at

different frequencies across the test session. After comparing the PSD contribution for each frequency range in *Pressers* and *Non-Pressers,* we observed that most of the signal was prevenient from the delta (0-4 Hz) and theta (4-10 Hz) bands, with a much smaller contribution coming from the alpha (10-14 Hz), beta (14-35 Hz), and gamma (>35 Hz) frequencies **(Fig. 4A)**. We therefore focused our analyses on these two bands and found that *Pressers* displayed increased power in the delta band, whereas *Non-Pressers* exhibited increased power in the theta band during the three phases of the test session **(Fig. 4B-C)**. Differences between *Pressers* and *Non-Pressers* were also observed in the time-frequency domain through changes in the log of PSD for delta and theta bands across the different phases **(Fig. 4D-E)**. These results indicate that phenotypic differences in approach-avoidance conflict are associated with distinct oscillatory frequencies in PL.

In pressers, PL^{GLUT} neurons show reduced spontaneous activity during the conflict phase.

The rodent mPFC, including PL, is primarily composed of excitatory glutamatergic cells that correspond to 75-85% of the neurons in this area. In contrast, inhibitory GABAergic interneurons comprise 15-25% of the local neurons (Santana et al., 2004; Gabbott et al., 2005). Previous studies have shown that PL glutamatergic (PL^{GLUT}) neurons are necessary for the retrieval of conditioned threat responses (Do-Monte et al., 2015), whereas PL GABAergic (PL^{GABA}) neurons are implicated in both the encoding and the retrieval of threat associations by regulating the firing rate of PL^{GLUT} neurons (Courtin et al., 2014; Cummings and Clem, 2020). In addition, during foraging

in a safe context, food-associated cues activate both PL^{GLUT} and PL^{GABA} neurons (Burgos-Robles et al., 2013; Gaykema et al., 2014), and inactivation of PL^{GLUT} neurons may increase or reduce conditioned food-seeking responses depending on the specific downstream projections that are being modulated (Otis et al., 2017). While these studies suggest a role for both PL^{GLUT} and PL^{GABA} neurons in the regulation of threat and food-seeking responses in isolation, it remains unexplored how these two subsets of PL neurons regulate the trade-off between seeking rewards and avoiding potential threats during a conflict situation. To address this question, we combined single-unit recordings with optogenetics to track the neuronal activity of photoidentified PL^{GLUT} and PL^{GABA} neurons during the test session.

For photoidentification of PL^{GLUT} neurons, we injected into PL a viral vector (AAV-CaMKIIα-hChR2-(H134R)-eYFP) with a gene promoter (CaMKIIα) that favors the expression of the light-activated cation channel channelrhodopsin (ChR2) in PL^{GLUT} neurons. This CaMKIIα labeling approach has been successfully used in previous studies (Gradinaru et al., 2009; Tye et al., 2011) and was validated here for PL neurons by showing a lack of immunocolabeling between the viral vector and the GABAergic marker GAD67 **(Fig. 5A)**. Rats expressing ChR2 selectively in PL^{GLUT} neurons were implanted with an optrode into the same region for optogenetic-mediated identification of PL^{GLUT} neurons at the end of the behavioral session **(Fig. 5B)**. Among the recorded PL cells, 39 out of 104 neurons (n = 5 rats) showed short-latency responses (< 6 ms) to laser illumination and were classified as PL^{GLUT} neurons **(Fig. 5C-D** and Methods**)**. Previous studies have shown that photoactivation of PL^{GLUT} neurons can lead to indirect activation of synaptically connected neurons in the region, but these indirect responses

to laser illumination in cortical regions take longer than 9 ms to occur (Lima et al., 2009). For photoidentification of PL^{GABA} neurons, we injected into PL a viral vector (AAV-mDlx-ChR2-mCherry) with a gene promoter (mDlx) that favors the expression of ChR2 in PL^{GABA} neurons. This mDlx labeling approach has been successfully used in previous studies (Dimidschstein et al., 2016; Sun et al., 2020), and was validated here for PL neurons by using two different methods: an immunohistochemical approach that resulted in significant immunocolabeling between the viral vector and the GABAergic marker GAD67 **(Fig. 5E)**, and an *in situ* hybridization approach which confirmed that ~88% of the cells labeled with the viral vector also expressed the GABAergic marker vGAT **(Supplementary Fig. 4A-B)**. Rats expressing ChR2 selectively in PL^{GABA} neurons were implanted with an optrode into the same region for optogenetic-mediated identification of PL^{GABA} neurons at the end of the behavioral session **(Fig. 5F)**. Among the recorded PL cells, 84 out of 338 neurons (n = 19 rats) showed short-latency responses to laser illumination (< 12 ms) and were classified as PL^{GABA} neurons **(Fig. 5G-H and Methods)**. A longer latency criterion was used for GABAergic neurons because indirect photoactivation of neighboring cells would require a disinhibitory mechanism that has been shown to take longer than 15 ms in cortical regions (Pi et al., 2013).

After separating the photoidentified cells into PL^{GLUT} and PL^{GABA} neurons, we aligned their activities to the onset of the food cues and compared changes in firing rates from the reward to the conflict phase in *Pressers* **(Fig. 5I)**. We observed that the proportions of excitatory and inhibitory food cue responses for PL^{GLUT} and PL^{GABA} neurons were similar during the reward and the conflict phases **(Fig. 5J-K)**. Next, we

analyzed the spontaneous activity of PL^{GLUT} and PL^{GABA} neurons and compared changes in their firing rates across the different phases of the test session **(Fig. 5L)**. We found that the average firing rate of PL^{GLUT} neurons remained the same across the different phases of the test (~5 Hz; **Fig. 5M**), with most of the cells (53%) changing their activities in more than one session **(Fig. 5N)**. A group analysis of the firing rates across phases demonstrated that PL^{GLUT} neurons were disinhibited during the odor phase, and subsequently inhibited during the conflict phase when *Pressers* resumed searching for food **(Fig. 5O)**. Similar to PL^{GLUT} neurons, the average firing rate of PL^{GABA} neurons also remained the same across the different phases of the test (~8 Hz, **Fig. 5P)**, with most of the cells (65%) changing their activities in more than one session **(Fig. 5Q)**. However, in contrast to PL^{GLUT} neurons, a group analysis of the firing rates of PL^{GABA} neurons did not reveal significant differences across the phases **(Fig. 5R)**. Because PL is comprised of different subpopulations of interneurons that inhibit each other during food seeking or defensive responses (Gaykema et al., 2014; Cummings and Clem, 2020), we cannot rule out the possibility that distinct subsets of PL^{GABA} neurons were preferentially recruited during each one of the phases.

To evaluate how the spontaneous activity of the same PL neurons changed during the test session, we tracked the firing rate of PL^{GLUT} and PL^{GABA} neurons across the different phases. We found that all PL^{GLUT} neurons that were either excited or inhibited during the reward phase responded in opposite direction or did not change their activities during the odor phase **(Supplementary Figure 5A-B)**, suggesting the existence of distinct subpopulations of PL^{GLUT} neurons that encode valence-specific information. In contrast, no significant differences in the proportions of excitation and

inhibition were observed in PL^{GABA} neurons during the transition from reward to odor phase nor during the transition from odor to conflict phase for both subsets of PL neurons **(Supplementary Figure 5C-F)**. Furthermore, both PL^{GLUT} and PL^{GABA} neurons showed the same proportion of excitatory and inhibitory responses during the onset of freezing, avoidance, or risk-assessment behaviors **(Supplementary Figure 6A-C)**, indicating that both subsets of PL neurons may contribute to the expression of distinct defensive responses during conflict. Together, our data suggest that PL^{GLUT} neurons are disinhibited when foraging rats exhibit increased defensive behaviors in response to the conditioned odor and become inhibited again when animals resume searching for food during the conflict phase.

Putative classification of PL neurons based on spike waveform and spike timing parameters is insufficient to differentiate glutamatergic and GABAergic cells

Previous single-unit recording studies have used an indirect cluster analysis of spike waveform and spike timing parameters to classify neurons into putative glutamatergic or putative GABAergic cells (Hassani et al., 2009; Courtin et al., 2014; Fan et al., 2017). While it is widely accepted that glutamatergic neurons exhibit longer spike duration and lower firing rate than GABAergic neurons (Mruczek and Sheinberg, 2012; Ono et al., 2017), a direct comparison between optogenetic photoidentification and putative classification of PL neurons *in vivo* is currently missing to confirm that extracellular spike parameters can be reliably used to separate glutamatergic and GABAergic cells.

We sought to address this question by extracting the extracellular spiking properties of the 123 photoidentified PL neurons shown in **Figure 5** and plotting their values to perform a cluster analysis separation. Because the amplitude of the waveform has been shown to directly correlate with the distance between the recording electrode and the neuronal soma (Weir et al., 2014), we limited our analyses to the duration of the action potentials (i.e., spike half-width) and the firing rate of the neurons (i.e., frequency), similar to previous putative classifications *in vivo* (Frank et al., 2001; Constantinidis and Goldman-Rakic, 2002; Bartho et al., 2004). Using an unbiased unsupervised cluster-separation algorithm, we separated the cells into putative PL^{GLUT} and putative PL^{GABA} neurons based on spike waveform and spike timing features by using k-means++ algorithm as a heuristic to find centroid seeds for k-means clustering (see Methods for details). Only *in vivo* photoidentified GABAergic or glutamatergic neurons were considered for this analysis. The spike half-width feature was the driving force for the classification and indicated a division of clusters at ~0.175 ms **(Supplementary Figure 7A)**. By marking the cells that were previously photoidentified as PL^{GLUT} or PL^{GABA} neurons on the same cluster distribution, we calculated the percentage of PL^{GLUT} or PL^{GABA} neurons that were correctly identified with the putative classification **(Supplementary Figure 7A-B)**. Surprisingly, we observed less than 40% of overlapping between the optogenetic photoidentification and the putative analysis **(Supplementary Figure 7B-C)**, indicating that cell-type putative classification of glutamatergic and GABAergic neurons in PL should be treated with caution. These results are consistent with prior studies *in vivo* showing that pyramidal and inhibitory neurons exhibit a wide variety of frequencies and spike durations, which alone may not

be sufficient for putative cell-type classification (Vigneswaran et al., 2011; Becchetti et al., 2012; Weir et al., 2014).

Photoactivation of PL^{GLUT}, but not PL^{GABA} neurons, suppresses reward-seeking responses.

To further establish whether changes in the activity of PL neurons can alter cue-triggered food-seeking responses, we used an optogenetic approach to selectively activate either PL^{GLUT} or PL^{GABA} neurons during a cued food-seeking test in a neutral context. We initially infused either the viral vector AAV-CaMKIIα-ChR2-eYFP **(Fig. 6A)** or AAV-mDlx-ChR2-mCherry **(Fig. 6E)** into PL and implanted an optrode into the same region to examine how photoactivation of PL^{GLUT} or PL^{GABA} neurons change local activity. Laser illumination of PL^{GLUT} somata increased the firing rate of most responsive PL neurons (9 out of 20 neurons, 45%), with some neurons showing reduced activity (6 out of 20 neurons, 30%, **Fig. 6B-D**). Neurons that increased their activities showed shorter response latencies (2.1 ±0.24 s) compared to neurons that reduced their activities (41.3 ± 5.57 s), suggesting direct responses (i.e., opsin-mediated) versus indirect responses (i.e., multi-synaptic), respectively. Conversely, laser illumination of PL^{GABA} somata reduced the firing rate of all responsive PL neurons (16 out of 22 neurons, 73%; **Fig. 6F-H)**, indicating a suppression in local activity. After investigating the local effects of photoactivating either PL^{GLUT} and PL^{GABA} neurons, we infused another set of animals with the same viral vectors in PL and implanted bilateral optical fibers into the same region to manipulate PL activity during the cued food-seeking test **(Fig. 6I-J)**. Rats expressing only eYFP in PL were used to control for any nonspecific

effects of viral transduction or laser heating. To assess the effects of PL photoactivation on lever presses, we alternated two trials of food cues with the laser on vs. laser off conditions **(Fig. 6K-L)**. Photoactivation of PL^{GLUT} (CaMKIIα-ChR2), but not PL^{GABA} (mDlx-ChR2) neurons, reduced the frequency of lever presses **(Fig. 6M)** and increased the latency for the first press after the cue onset **(Fig. 6N)**, when compared to control group. Photoactivation of either PL^{GLUT} or PL^{GABA} neurons did not induce freezing behavior **(Fig. 6O)**. These results are consistent with our electrophysiological recordings in **Fig. 5O** showing that increased inhibition in the firing rate of PL^{GLUT} neurons correlates with augmented reward-seeking responses during conflict. Overall, these findings suggest that increasing the activity of PL^{GLUT} neurons is sufficient to suppress cued reward-seeking responses in a neutral context.

Photoinhibition of PL^{GLUT} neurons in *Non-pressers* reduces freezing responses and increases food approaching during conflict.

Our electrophysiological experiments in **Fig. 5O** demonstrate that PL^{GLUT} neurons are disinhibited when rats express defensive responses to the conditioned odor. In addition, our photoactivation experiments in **Fig. 6K-O** indicate that increasing the activity of PL^{GLUT} neurons suppresses cued reward-seeking behavior in rats that are pressing a lever for food. We next hypothesized that photoinhibition PL^{GLUT} neurons during conflict would attenuate defensive behaviors and rescue food-seeking responses in *Non-Pressers*. To test this hypothesis, we injected a group of rats with the viral vector AAV-CaMKIIα-eNpHR-eYFP (or AAV-CaMKIIα-eYFP) into PL to express the inhibitory opsin halorhodopsin (or eYFP control) selectively in PL^{GLUT} neurons **(Fig. 7A)**. Rats were

initially exposed to a cued food-seeking test to assess the effects of photoinhibition of PL^{GLUT} neurons on food-seeking responses in a neutral context. We observed that photoinhibition of PL^{GLUT} neurons had no effect on lever pressing rate, latency to press the lever or freezing responses before threat conditioning **(Supplementary Fig. 8A-E)**. Animals were then threat conditioned as in **Fig. 1** and on the following day exposed to the odor arena for a test session. During the conflict phase, the first pair of food cues was used to classify the animals into *Pressers* and *Non-Pressers*, whereas the subsequent pairs of food cues were alternated between laser on and laser off conditions to assess the effects of illumination of PL^{GLUT} neurons on approach-avoidance responses **(Fig. 7B-C)**. Remarkably, photoinhibition of PL^{GLUT} neurons (CaMKIIα-eNpHR) in *Non-Pressers* reduced the percentage of time rats spent freezing **(Fig. 7D)** and avoiding the odor area **(Fig. 7E)**, and increased the percentage of time rats spent approaching the food area **(Fig 7F)** during the food cue presentation, when compared to the eYFP-control group. Despite the increase in food approaching behavior, photoinhibition of the same cells had no effects on lever pressing responses **(Fig. 7G-H)**. In another subset of *Non-Presser* rats, photoactivation of PL^{GABA} neurons (mDlx-ChR2) did not alter food seeking nor defensive responses during the conflict phase, when compared to the mCherry-control group **(Fig 7I-P)**. Taken together, these results demonstrate that reduced activity in PL^{GLUT} neurons during conflict situations reduces defensive responses and biases rats' behavior toward food seeking.

DISCUSSION

Using a novel approach-avoidance conflict test, we demonstrated that PL neurons regulate reward-approach vs. threat-avoidance responses during situations of uncertainty, when rats use previously associated memories to guide their decisions. We found that increased risk-taking behavior in *Pressers* was associated with a larger number of food-cue responses in PL neurons, which were higher in magnitude and persisted during the conflict phase, when compared to *Non-Pressers*. In addition, PL^{GLUT} neurons showed reduced spontaneous activity during risky reward seeking and photoactivation of these cells in a neutral context was sufficient to suppress lever press responses. Accordingly, photoinhibition of PL^{GLUT} neurons at the onset of the food cues in *Non-Pressers* reduced defensive responses and increased food-approaching during the conflict phase, consistent with our observation that a small fraction of PL neurons changed their activity at the onset of freezing, avoidance or risk-assessment responses. Altogether, these results suggest that under memory-based conflict situations, reduced or increased activity in PL^{GLUT} neurons can favor the behavioral expression of food-approaching or threat-avoidance responses, respectively.

During our approach-avoidance conflict test, *Pressers* and *Non-Pressers* showed similar levels of lever pressing before the conflict phase (e.g., cued food-seeking training, threat conditioning, and reward phases). This observation suggests that these two individual phenotypes most likely emerged during the test session and were independent of prior differences in sucrose preference or food-seeking motivation. Similarly, because both groups exhibited the same percentage of freezing during the olfactory threat conditioning session, the increased defensive behaviors and the

481 reduced food-seeking responses observed in *Non-Pressers* during the test session
482 were unlikely due to higher acquisition of conditioned threat responses. Furthermore,
483 other external factors such as shock sensitivity or pain tolerance cannot be accounted
484 for the individual differences observed in our experiments because both groups reacted
485 equally to the unconditioned stimulus (i.e., velocity measured as maximum speed after
486 the footshocks) and, different from other conflict tasks using footshocks as a
487 punishment during the conflict test (Geller, 1960; Vogel et al., 1971; Oberrauch et al.,
488 2019), in our model rats were not exposed to footshocks during the conflict phase.
489 Therefore, the most plausible interpretation for the behavioral differences observed in
490 our task is that *Pressers* and *Non-Pressers* have allocated distinct motivational
491 significance to the food- or shock-paired cues during the test session.

492 Individual differences in risky decision making have also been reported in other
493 studies using rodent models of behavioral conflict involving footshock punishment
494 (Simon et al., 2009; Jean-Richard-Dit-Bressel et al., 2019; Bravo-Rivera et al., 2021),
495 reversal learning (Bari et al., 2010), or variations in reward probability (Ainslie, 1975; St
496 Onge and Floresco, 2009; Dellu-Hagedorn et al., 2018), although the neural
497 mechanisms underlying such differences are less clear. Evidence indicates that some of
498 the neurobiological bases of individual variation in stimulus-reward response depend on
499 differences in dopamine levels in subcortical circuits (Tomie et al., 2000; Flagel et al.,
500 2007; Flagel et al., 2011), which are regulated by top-down mechanisms involving the
501 mPFC (Ferenczi et al., 2016; Haight et al., 2017; Serrano-Barroso et al., 2019).
502 Accordingly, our neural correlate analyses of risk-taking vs. risk-avoiding behaviors in
503 the PL subregion of the mPFC revealed some clear differences between the two

phenotypes, suggesting that PL neurons participate in behavioral selection when rats' decision depends on the conflicting memories of reward and threat. One interesting finding in our study was the observation that *Pressers* showed a larger number and a higher magnitude of food-cue responses during the conflict phase when compared to *Non-Pressers*, indicating that PL neurons can differentiate between situations involving motivational conflict and those that do not. Because PL neurons are known for encoding the value of reward-predictive cues (Sharpe and Killcross, 2015; Otis et al., 2017), the increase in the number and magnitude of food cue responses observed in *Pressers* might result in a greater allocation of attention to food cues, which would explain the persistent reward-seeking responses observed in this group during motivational conflict. In support of this interpretation, reward-paired cues can acquire motivational salience in some subjects and become sufficient to elicit reward-seeking responses in both rodents (Robinson and Flagel, 2009; Robinson et al., 2014) and humans (Smith et al., 2011; Jensen and Walter, 2014). Consistently, *Pressers* also showed a larger number and a higher magnitude of food cue responses in PL before the conflict phase (i.e., reward phase), although the percentage of rewarded presses and the latency to press the lever during the reward phase were similar between the two groups.

Another possible interpretation for the differences in food-cue responses in *Pressers* and *Non-Pressers* is the reduced excitatory-food cue responses in *Non-Pressers,* which may be mediated by cue-evoked inhibitory inputs to PL during the conflict phase. While the source of this inhibition is unclear, a potential candidate are GABAergic neurons in the ventral tegmental area (VTA^{GABA}), which correspond to 35% of the cells in this region and send significant projections to PL (Nair-Roberts et al.,

2008; Breton et al., 2019). Previous studies have shown that VTA^{GABA} neurons change their firing rates in response to reward-predicting cues (Cohen et al., 2012), and chemogenetic activation of these cells suppress the activity of local dopaminergic neurons (van Zessen et al., 2012), reduces cue-evoked sucrose-seeking responses (Wakabayashi et al., 2019), and induces conditioned place aversion in rodents (Tan et al., 2012). Future studies need to determine whether this regulation of rewarding and aversive responses by VTA^{GABA} neurons can also be attributed to their long-range inhibitory projections to PL neurons, particularly during conflict situations.

Differences in risk-taking and risk-avoiding behaviors were also reflected on LFP frequencies in PL neurons in the beginning of the test session, with *Pressers* and *Non-Pressers* displaying increased power in the delta or theta bands, respectively. These findings are in corroboration with previous studies showing that increased delta power activity in the mPFC is associated with both reward-seeking and preparatory attention (Horst and Laubach, 2013; Totah et al., 2013; Emmons et al., 2016), whereas augmented theta power in the mPFC or synchronized theta activity between mPFC and BLA is correlated with the expression of avoidance responses or the consolidation of threat memories, respectively (Popa et al., 2010; Padilla-Coreano et al., 2019). More specifically, increased synchrony between mPFC and BLA activity in the theta frequency range has been reported for animals that successfully differentiate between aversive and safe cues (or environments) during a differential threat conditioning task (or an open field arena) (Likhtik et al., 2014; Stujenske et al., 2014). In addition, prior studies have shown that 4 Hz LFP oscillations in the mPFC and BLA were strongly synchronized during conditioned freezing episodes (Courtin et al., 2014; Dejean et al.,

2016; Karalis et al., 2016), and these sustained 4 Hz oscillations in the mPFC were independent of hippocampal low-theta oscillations, suggesting that they were internally generated in the mPFC during the expression of freezing behavior (Karalis et al., 2016). Consistent with these findings, in our study *Non-Pressers* showed increased theta activity and marked 4 Hz oscillations in PL neurons, which were associated with better discrimination between reward and threat cues and increased freezing responses during the test session, when compared to *Pressers*.

Increased risk-taking behavior in *Pressers* was associated with a higher number of PL^{GLUT} neurons showing reduced spontaneous activity during the conflict phase. In contrast, risk-avoiding responses in *Non-Pressers* were associated with increased spontaneous activity during conflict. While this set of results suggest that distinct patterns of PL activity are associated with risk-taking or risk-avoiding behaviors in conflict situations, our optogenetic manipulation provided a causal role for PL^{GLUT} neurons in the regulation of approach-avoidance conflict. For instance, the reduction in food-seeking responses during photoactivation of PL^{GLUT} neurons indicates that increased activity in PL pyramidal cells is sufficient to recapitulate the reward-seeking suppression observed during conflict. Our findings agree with previous studies showing that increased activity in mPFC neurons, including PL, attenuates reward-seeking responses in a neutral context (Berglind et al., 2007; Chen et al., 2013; Ferenczi et al., 2016; but see: Warthen et al., 2016), an effect that has been attributed, at least in part, to downstream projections to the paraventricular nucleus of the thalamus (PVT) (Otis et al., 2017). Notably, PVT neurons are necessary for the retrieval of both reward- and threat-associated memories (for a review see: Do Monte et al., 2016; Millan et al., 2017;

573 McGinty and Otis, 2020; Penzo and Gao, 2021), and activity in PVT neurons has
574 recently been shown to be associated with the regulation of approach-avoidance
575 responses during situations of conflict (Choi and McNally, 2017; Choi et al., 2019;
576 Engelke et al., 2021), suggesting a potential target by which PL glutamatergic neurons
577 may exert their effects.

578 Considering that *Pressers* showed a higher number of excitatory food-cue
579 responses than *Non-Pressers*, it is counterintuitive that photoactivation of PL^{GLUT}
580 neurons during the food cue onset resulted in reduced food-seeking responses.
581 However, it is important to note that our optogenetic manipulation not only altered the
582 activity of food-cue responsive neurons, but mostly the global activity of other PL^{GLUT}
583 neurons. Thus, it is possible that increased activity in the firing rate of PL^{GLUT} neurons
584 may result in reduced signal-to-noise ratio during the food cue onset (Kroener et al.,
585 2009; McGinley et al., 2015), and consequently decreased food-seeking responses. In
586 contrast, by reducing their spontaneous firing rates during conflict situations, PL^{GLUT}
587 neurons become more likely to fire in response to food cues due to an increase in the
588 signal-to-noise ratio, thereby resulting in persistent reward-seeking responses during
589 the conflict phase as we propose in our schematic in Fig. 8.

590 Additionally, our findings showing that inactivation of PL^{GLUT} neurons increases
591 food-approaching responses in *Non-Pressers* suggest that PL activity is indispensable
592 to inhibit reward pursuit in the presence of threat-associated cues. The lack of effects on
593 lever pressing may indicate that other parallel brain regions may be modulating the
594 suppression of operant lever-press responses during conflict. Alternatively,
595 photoinhibition of PL^{GLUT} neurons was not large enough to produce a more global effect

on risky behavior (i.e., completely restore lever presses). Collectively, these results add to a growing literature indicating that PL neurons are necessary to guide appropriate food-seeking behavior in tasks that rely on discrimination among environmental cues (Marquis et al., 2007; Sangha et al., 2014; Moorman and Aston-Jones, 2015) or decision-making tasks involving risk of punishment in which animals need to: i) adapt choice behavior during shifts in risk contingencies (Orsini et al., 2018), ii) regulate behavioral flexibility (Radke et al., 2015; Capuzzo and Floresco, 2020), or iii) suppress reward seeking in response to conditioned aversive stimuli (Kim et al., 2017; Piantadosi et al., 2020). Moreover, our results are in accordance with previous findings demonstrating that inactivation of PL neurons, or their inputs from BLA, increases risk-taking behavior in a conflict task in which rats needed to refrain from consuming sucrose to avoid a footshock (Burgos-Robles et al., 2017; Verharen et al., 2019).

Previous studies have shown that PL neurons fire in response to shock-paired cues and such activity is highly correlated with the expression of freezing responses (Burgos-Robles et al., 2009; Sotres-Bayon et al., 2012; Kim et al., 2013; Courtin et al., 2014). Adding to these findings, our recordings demonstrated that the activity of a small number of PL neurons correlated with the onset of freezing responses, with the same proportion of freezing-responsive cells being classified as PL^{GLUT} or PL^{GABA} neurons (~10%). At first sight, the lack of effects on freezing behavior following optogenetic activation of PL^{GLUT} neurons seems at odds with our recordings. It also seems to disagree with previous studies showing that electrical stimulation or optogenetic induction of 4Hz oscillations in PL increases conditioned freezing responses (Vidal-Gonzalez et al., 2006; Courtin et al., 2014) by synchronizing the neural activity between

PL and BLA regions (Karalis et al., 2016). However, one important difference between our study and others is that photoactivation of PL^{GLUT} neurons in our experiments was performed in naïve rats, in the absence of shock-paired cues. Thus, the increased freezing responses following PL activation reported in previous studies appear to be dependent on the preexistence of a conditioned threat memory.

Overall, our results outline the neural correlates of risk-taking and risk-avoiding behaviors in PL and reveal an important role for PL^{GLUT} neurons in coordinating memory-based risky decision-making during conflict situations. Further studies will focus on identifying the PL downstream/upstream circuits that regulate reward-approaching and threat-avoidance responses, as well as the potential genetic and epigenetic factors that could contribute to the observed behavioral phenotypes. Elucidating the underlying mechanisms that mediate risk-taking vs. risk-avoiding responses during situations of uncertainty may help to provide understanding of response selection and adaptive behaviors, and may have clinical relevance to many psychiatric disorders (Aupperle and Paulus, 2010; Kirlic et al., 2017). Whereas persistent avoidance of presumed threats is the cardinal symptom of anxiety disorders (Treanor and Barry, 2017), seeking reward despite negative consequences is a hallmark of both eating and substance use disorders in humans (Volkow et al., 2012).

ACKNOWLEDGEMENTS

We thank Dr. Roger Janz for helping us with the packaging of the AAV-mDLX-ChR2-mCherry viral construct, and Maria Nasheed, Ryia Albert and Sharon Gordon for their technical assistance. We also thank current and former members of the Do Monte and

Quirk Labs for their valuable comments on the manuscript, and the Mind the Graph team for creating the schematic drawings presented in the manuscript. This work was supported by NIH grants R00-MH105549 and R01-MH120136, a Brain & Behavior Research Foundation grant (NARSAD Young Investigator), and a Rising STARs Award from UT System to F.H.D-M.

Author contributions

J.A.F-L., D.S.E., and G.A.M. performed the behaviors, optogenetics, and single-unit recordings. D.S.E. carried out the immunohistochemical and *in situ* hybridization studies. A.G. wrote and validated the DeepLabCut and the Python codes for behavioral analyses. J.A.F-L. wrote the MATLAB and Python codes for single-unit recording analyses. Both J.A.F-L. and F.H.D-M. analyzed the single-unit recording data. D.S.E. performed the statistical analyses. All the authors helped to design the study and interpret the data. J.A.F-L. and F.H.D-M. prepared the manuscript with comments from all the co-authors.

Competing interests

The authors declare no competing interests.

Correspondence and requests for materials should be addressed to F.H.D-M.

METHODS

Animals. All experimental procedures were approved by the Center for Laboratory Animal Medicine and Care of The University of Texas Health Science Center at Houston. The National Institutes of Health guidelines for the care and use of laboratory animals were strictly followed to minimize any potential discomfort and suffering of the animals. Male Long-Evans hooded adult rats (Charles Rivers Laboratories) with 3-5 months of age and weighing 300-450 g at the time of the experiment were used. Rats were single-housed and after a 3-day acclimation period handled and trained to press a lever for sucrose as described below. Animals were kept in a 12-hour light/12-hour dark cycle (light from 7:00 to 19:00) and maintained on a restricted diet of 18 g of standard laboratory rat chow provided daily at end of experimentation. Animals were given *ad libitum* access to water. Animals' weights were monitored weekly to ensure all animals maintained their weight under food restriction. During pre- and post- surgery phases, animals were given *ad libitum* access to food for a total of 7 days.

Surgeries. Rats were anaesthetized with 5% isoflurane in an induction chamber. Animals were positioned in a stereotaxic frame (Kopf Instruments) and anesthesia was maintained with 2.5% isoflurane delivered through a facemask. A heating pad was positioned bellow the body of the animal and both temperature and respiration were monitored during the entire surgery. Veterinary lubricant ointment was applied on the eyes to avoid dryness during the surgery. Animals received a subcutaneous injection of the local anesthetic bupivacaine (0.25%, 0.3 ml) at the incision site. Iodine and ethanol (70%) were alternately applied for asepsis of the incision site. The surgery procedures varied according to the type of implantation/injection (see below). For injection-only

surgeries, the incision was stitched after the injection by using surgical suture (Nylon, 3-0). For implantation surgeries, the implants were fixed to the skull using C&B metabond (Parkell), ortho acrylic cement, and four to six anchoring screws. After surgery, animals received a subcutaneous injection of meloxicam (1 mg/Kg) and a topical triple antibiotic was applied to the incision area.

Viral vector injection. Viral injections were performed using a microsyringe (SGE, 0.5 µl) with an injection rate of 0.04 µl/min plus an additional waiting time of 12 min to avoid back-flow. The adeno-associated virus (AAV) was bilaterally injected at a volume of 0.4 µl per side. The AAV-CaMKIIα-eNpHR-eYFP vector was used to inhibit glutamatergic neurons, whereas AAV-mDlx-ChR2–mCherry or AAV-CaMKIIα-ChR2-eYFP vectors were used to activate either GABAergic or glutamatergic neurons, respectively. The use of mDlx or CaMKIIα promoters enabled transgene expression favoring either GABAergic or glutamatergic neurons, as previously shown (Gradinaru et al., 2009; Tye et al., 2011; Dimidschstein et al., 2016; Sun et al., 2020) and was confirmed by our immunohistochemical and RNAscope assessment **(Supplementary Fig. 4)**. The viral construct AAV-CaMKIIα-eYFP was used to control for any nonspecific effects of viral infection or laser heating. All plasmid or viral vectors were obtained from Addgene or University of North Carolina Viral Vector Core. For implantation of optrodes, the following coordinates from bregma were used for virus injection: PL, +2.7 mm AP, ±0.7 mm ML, -3.8 mm DV at a 0º angle. For PL soma illumination, an optical fiber (0.39 NA, 200 nm core, Inper) was implanted in each hemisphere targeting PL neurons using the following coordinates from bregma: +2.7 mm AP; ±1.5 mm ML; -4.0 mm DV at a 15º angle.

Single-unit electrodes. An array of 16 or 32 microwires was unilaterally implanted targeting the PL using the following coordinates from bregma: +2.7 mm AP, ±0.8 mm ML, -3.9 mm DV. Three different electrode configurations were used: i) 32-channel silicon probes (Buzsaki32-CM32 or A1x32-5mm-25-177-CM32, Neuro Nexus Technologies, USA), ii) Micro-Wire Arrays (MWA) of 16 or 32 channels (Bio-Signal Technologies Ltd, USA); or iii) custom designed electrodes with 2×8 grid with 150 µm of space between wires, 200 µ of space between rows, with 35 µm diameter wires (Innovative Neurophysiology Inc., USA). For photoidentification of GABAergic or glutamatergic neurons, a Hermes 32 channels optrode array was used (200 nm core, Bio-Signal Technologies Ltd). Optrodes were unilaterally implanted at the same coordinates described above after the infusion of 0.6 µl of AAV-mDlx-ChR2–mCherry or AAV-CaMKIIα-ChR2-eYFP vectors. In all cases, the ground wire was wrapped around a grounding screw previously anchored into the skull. Two insulated metal hooks were implanted bilaterally into the cement to allow firmly attachment of the array connector to the cable during recording.

Odor preparation. A 99% amyl acetate solution (Sigma Aldrich) was diluted in propylene glycol (Bluewater Chemgroup, Inc) to a 10% solution and presented to the rats during the different stages and phases of the olfactory threat conditioning test. A customized olfactometer (Med Associates) was used to control the flow of air into the animal's chamber. Before being mixed with the 10% amyl acetate solution, the air was passed through a desiccant and a charcoal filter to remove any moisture and odors, and was finally rehydrated with distilled water before being delivered into the chamber

734 through a thermoplastic PVC-based tube (Tygon) attached to an odor port located in the
735 odor area.

736 **Behavioral Tasks**

737 *Lever-press training.* Rats were placed in a plexiglass, standard operant box (34 cm
738 high x 25 cm wide x 23 cm deep, Med Associates), and trained to press a lever for
739 sucrose on a fixed ratio of one pellet for each press. Next, animals were trained in a
740 variable interval schedule of reinforcement that was gradually reduced across the days
741 (one pellet every 15 s, 30 s, or 60 s) until the animals reached a minimum criterion of 10
742 presses/min. All sessions lasted 30 min and were performed on consecutive days.
743 Sucrose pellet delivery, variable intervals, and session duration were controlled by an
744 automated system (ANY-maze, Stoelting). Lever-press training lasted approximately
745 one week, after which animals were assigned to surgery or cued food-seeking training.
746 A small number of rats failed to reach the lever press criteria and were excluded from
747 the experiments (< 3%).

748 *Cued food-seeking training.* Rats previously trained to press a lever for sucrose were
749 trained to learn that each lever press in the presence of an audiovisual cue (tone: 3
750 KHz, 75 dB; light: yellow, 2.8 W; 30 s duration) resulted in the delivery of a sucrose
751 pellet into a nearby dish. Reward cue conditioning also took place in the standard
752 operant boxes. While the light cue helps to direct the animals toward the lever during
753 the beginning of the training phase, the tone assures that the animals will not miss the
754 presentation during the trial and provides the temporal precision required for single-unit
755 recordings. After ~4 consecutive days of training (24 trials per day, pseudorandom
756 intertrial interval of ~120 s, 60 min session), rats learned to discriminate the food-

757 associated cue as indicated by a significant increase in press rate during the presence
758 of the audiovisual cues, when compared to the 30 s immediately before the cue onset
759 (cue-off, see **Supplementary Fig. 1A**). The cued food-seeking training was completed
760 when animals reached 50% of discriminability index (presses during cue-on period
761 minus presses during cue-off period divided by the total number of presses). After the
762 cued food-seeking training was completed, rats with single-unit electrodes were
763 exposed to an additional training session in which the audiovisual cue ceased
764 immediately after the animals pressed the lever and a single sucrose pellet was
765 delivered into the dish. This extra training reduced the rat's response to a single press
766 and dish entry per cue, thereby enabling us to correlate each food-seeking event with
767 the neuronal firing rate by avoiding overlapping between consecutive events (e.g., lever
768 presses). The single-pellet training took place in the same plexiglass rectangular arena
769 subsequently used for the odor test (40 cm high x 60 cm wide x 26 cm deep, Med
770 Associates, see schematic in **Fig. 1A right**). The arena consisted of a hidden area (40
771 cm high x 20 cm wide x 26 cm deep) separated from an open area by a plexiglass
772 division. An 8-cm slot located in the center of the division enabled the animal to
773 transition between both sides of the arena. For behavioral quantification, the open area
774 was subdivided into a center area and a food area (40 cm high x 12 cm wide x 26 cm
775 deep), the latter containing a lever, a dish, and an external feeder similar to the food-
776 seeking operant box.

777 *Habituation day.* Animals were placed in the odor arena and exposed to 12 audiovisual
778 cues (30 s duration, pseudorandom inter-trial intervals of between 25-40 s) followed by
779 10 min of presentation to the neutral odor alone (10% amyl acetate) and an additional

12 audiovisual cues similar to the first cues but in the presence of the neutral odor delivered in the food area of the arena. Each lever press in the presence of the audiovisual cue resulted in the delivery of a sucrose pellet into the dish, and the audiovisual cue was ceased immediately after the animal pressed the lever.

Threat *conditioning day.* One day after the habituation day, rats were placed in a plexiglass, standard operant box similar to the cued food-seeking training box, but with the grid floor previously attached to a shock generator system. Rats were habituated to one nonreinforced odor presentation (10% amyl acetate, 30 s duration) followed by five odor presentations that coterminated with a foot shock (0.7 mA, 1 s duration, 258-318 s inter-trial intervals). An olfactometer system was used to precisely deliver the odor into the box (see odor preparation session above), whereas an exhaustor system was used to remove the odor from the box during the intertrial intervals. Between each odor presentation, audiovisual cues (30 s duration) signaling the availability of sucrose were presented to the animals. Each lever press during the audiovisual cues resulted in the delivery of a sucrose pellet into the dish. Shock grids and floor trays were cleaned with 70% ethanol between each rat.

Test day. One day after the threat conditioning session, rats were returned to the same arena used during the habituation and exposed to the exact same protocol. The first phase of the test session was called *reward phase* and the animals were exposed to 12 food cues. The second phase was called *odor phase* and the animals were exposed to 10 min of conditioned odor (10% amyl acetate) alone. The last phase was called *conflict phase* and the animals were exposed to 12 food cues in the presence of the conditioned odor. In order to press the lever for sucrose during the conflict phase, rats had to

803 approach the conditioned odor presented in the food area. After the end of the conflict
804 phase, the odor was extracted from the arena with an exhaustor and the floor and walls
805 of the arena were cleaned thoroughly with 70% ethanol solution.

806 **Behavioral tracking.** Both the standard operant boxes and the testing arenas were
807 equipped with video cameras and a behavior tracking software (ANY-maze, Stoelting)
808 which were used to record the animal's behavior and control the delivery of sucrose,
809 foot shock, tone, light and odor in the apparatuses. Avoidance responses were
810 characterized by the time spent in the hidden area of the arena. Freezing responses
811 were characterized by the complete absence of movements except those needed for
812 respiration. Risk-assessment responses were characterized by a body stretching
813 movement to peep out toward the food area while in the hidden area and were used as
814 a measure of risk-assessment behavior (Blanchard et al., 2011).

815 For single-unit recording analyses, the detection of freezing, avoidance and risk
816 assessment behaviors were performed using the open source tool DeepLabCut, a
817 machine learning software that tracks complex patterns of behavior from videos (Mathis
818 et al., 2018). After a video has been analyzed, the data was saved to a .csv file that
819 contained the x and y location of each rat's body part in pixels, as well as the analysis of
820 the expected accuracy (i.e., likelihood) of the tracked positions across time. After
821 DeepLabCut has calculated the positions and the likelihood, we used three different
822 Python codes to identify each one of the three behaviors. For freezing behavior, the
823 code used DeepLabCut's position data and determined if the rat was still for more than
824 500 ms. The animal was considered to be still if the position in question was within 1.05
825 pixels of each other. For avoidance behavior, the code used DeepLabCut's position

826 data to determine the location of the rat in the arena and based on the center of its head
827 to identify when the animals entered the hidden area of the arena. Finally, for risk
828 assessment behavior, the code used DeepLabCut's position data to identify the nose,
829 ears, center of the head, and spine to determine whether the rat was located in the
830 hidden area of the arena with its body stretched and the head looking through the open
831 division of the apparatus. Each of these codes generated a .xlsx file that contained the
832 onset and the total duration of each behavioral episode. The time onsets for each
833 behavior were filtered by selecting only the events that lasted more than 1 second and
834 were not preceded by the same behavior during the previous 6 s (baseline). The final
835 list of time onsets was entered into the single-unit recording files to create the events
836 and temporally align them with the neuronal recordings.

837 **Optogenetic stimulation during behavior.** Bilateral optical cables (200 μm core, 0.37
838 NA, 2.5 mm ceramic ferrule, Inper) were connected to a blue laser (diode-pumped solid-
839 state, 473 nm, 150 mW output, OptoEngine) or a yellow laser (diode-pumped solid-
840 state, 593.5 nm, 300 mW output, OptoEngine) by using a patch cord (200 μm, 0.39 NA,
841 FC/PC connector, Inper) through a dual rotary joint (200 μm core, Doric lenses). During
842 the stimulation, the optical cables were coupled to the previously implanted optical
843 fibers by using a ceramic sleeve (2.5 mm, Precision Fiber Products). An optogenetic
844 interface (Ami-2, Stoelting) and an electrical stimulator (Master 9, A.M.P. Instruments)
845 were used to control the onset of the laser, pulse width, train duration, and frequency.
846 The power density estimated at the tip of the optical fiber was 7-10 mW for illumination
847 of PL somata (PM-100D, Power Energy Meter, Thor Labs).

Single-unit recording. A 64-channels neuronal data acquisition system (Omniplex, Plexon) integrated with a high-resolution video-tracking system (Cineplex, Plexon) was used for electrophysiological recordings from freely behaving animals. Both videos and neuronal recordings were combined within the same file, thereby facilitating the correlation of behavior with neuronal activity. An electrical isolation, Faraday cage was made and connected to the grounding port of the data acquisition system. The system was connected to the head-mounted electrode/optrode by using a digital headstage cable (32 channels, Plexon), a motorized carrousel commutator (Plexon), and a digital headstage processor (Plexon). Rats were habituated to the headstage cable daily for approximately one week before the beginning of the experiments. Extracellular waveforms exceeding a voltage threshold were band-pass filtered (500 - 5,000 Hz), digitized at 40 KHz, and stored onto disk. Automated processing was performed using a valley-seeking scan algorithm and then visually evaluated using sort quality metrics (Offline Sorter, Plexon). Single-units were selected based on three principal components and waveform features such as valley-to-peak and amplitude measurements. A commercial software (NeuroExplorer, NEXT Technologies), Matlab (MathWorks) scripts, and Python scripting in NeuroExplorer were implemented to calculate the spontaneous firing rate and food-cue responses. The spontaneous firing rate was calculated by comparing the frequency of spike trains during the last 30 s of the food-seeking phase, odor phase, or conflict phase against the 30 s prior to the beginning of each session. Food cue responses were calculated by implementing Matlab scripts as Z-scores normalized to 20 pre-cue bins of 300 ms. Neurons showing a Z-score > 2.58 ($p < 0.01$) during the first two-bins following the onset of the food cues

were classified as excitatory responses, whereas neurons showing a Z-score < -1.96 ($p < 0.05$) during the same first two-bins were classified as inhibitory responses. At the end of the recording sessions, a micro-lesion was made by passing anodal current (0.3 mA for 15 s) through the active wires to deposit iron in the tissue. After perfusion, brains were extracted from the skull and stored in a 30% sucrose/ 6% ferrocyanide solution to stain the iron deposits.

Photoidentification of PL neurons during recordings. During neuronal photoidentification, we recorded from rats expressing channelrhodopsin (ChR2) in PL neurons previously implanted with an optrode in the same region. An optical cable connected to a blue laser was attached to the headstage cable and coupled to the previously implanted optical fiber by using a ceramic sleeve. At the end of the behavioral session, 10 trains of 10-s blue laser pulses (5 ms pulse width, 5 Hz) were delivered by a Master-9 programmable pulse stimulator, which also sent flags to the data acquisition system to mark the time of the laser events. Neurons were considered to be responsive to photostimulation if they showed a significant increase in firing rate above baseline (20 ms, Z-score > 3.29, $p < 0.001$) within the 6 ms (for PL^{GLUT} neurons) or 12 ms (for PL^{GABA} neurons) after laser, similar to previous studies (Lima et al., 2009; Pi et al., 2013; Burgos-Robles et al., 2017; Engelke et al., 2021).

Optogenetic manipulation of PL neurons during behavior. During the cued food-seeking test, rats expressing ChR2 or eNpHR in PL were bilaterally illuminated in the same region by using a blue (5 ms pulse width, 5 Hz for CaMKIIα or 20 Hz for mDlx) or a yellow laser (constant illumination), respectively. The laser was activated at cue onset and persisted throughout the entire 30 s of the audiovisual cue presentation. Rats were

894 exposed to two consecutive cues with laser off followed by two consecutive cues with
895 laser on in a total of 12 cues (pseudorandom inter-trial intervals of between 25-40 s). To
896 assess the effects of PL illumination on rat's defensive behavior, PL neurons of rats
897 expressing ChR2 or eNpHR were bilaterally illuminated during 6 distinct epochs of 30 s
898 during the *odor phase* by using a blue (5 ms pulse width, 20 Hz) or a yellow laser
899 (constant illumination), respectively. To assess the effects of PL illumination on food-
900 seeking responses during the *conflict phase*, rats were exposed to two consecutive
901 cues with laser off followed by two consecutive cues with laser on in a total of 12 cues
902 (pseudorandom inter-trial intervals of between 25-40 s). The laser was activated at cue
903 onset and persisted on until the animal pressed the bar or the 30 s of the audiovisual
904 cue was completed.

905 **Histology.** Animals were transcardially perfused with KPBS followed by 10% buffered
906 formalin. Brains were processed for histology as previously described (Do-Monte et al.,
907 2013). Only rats with the presence of eYFP or mCherry labeling and the track of the
908 electrode wires or optical fiber tips located exclusively in PL were included in the
909 statistical analyses.

910 **Immunohistochemistry.** Rats previously infused with AAV-mDlx-ChR2-mCherry or
911 AAV-CaMKIIα-ChR2-eYFP were transcardially perfused with KPBS followed by 10%
912 buffered formalin. Brains were removed from the skull, transferred to a 20% sucrose
913 solution in KPBS for 24 h, and stored in a 30% sucrose solution in KPBS for another 24
914 h. Next, coronal PL sections (40 µm thick) were cut in a cryostat (CM 1860, Leica),
915 blocked in 20% normal goat serum and 0.3% Triton X-100 in KPBS at room
916 temperature for 1 h. For identification of GABAergic neurons, PL sections were

incubated with anti-GAD67 serum raised in rabbit (1:400; Millipore-Sigma) at 4°C for 48 h. After sections were washed in KPBS for 5 times, sections were incubated with a secondary anti-rabbit antibody (1:200, Alexa Fluor 488 or Alexa Fluor 594, Abcam) for 2 h. Sections were washed with KPBS, mounted in Superfrost Plus slides, and coverslipped with anti-fading mounting medium (Vectashield, Vectorlabs). Images were generated by using a microscope (Nikon, Eclipse NiE Fully Motorized Upright Microscope) equipped with a fluorescent lamp (X-Cite, 120 LED) and a digital camera (Andor Zyla 4.2 PLUS sCMOS).

***In situ* hybridization.** Single molecule fluorescent *in situ* hybridization (RNAscope Multiplex Fluorescent Detection Kit v2, Advanced Cell Diagnostics) was used following the manufacturer protocol for fixed-frozen brains sample. Brain samples were sectioned at a thickness of 20 µm in a cryostat (CM1860, Leica). Sections were collected onto superfrost plus slides (Fisher Scientific) and transferred to a −80°C freezer. To prepare for the assay, brain sections were serially dehydrated with EtOH (50%, 75%, and 100%, each for 5 min) and then incubated in hydrogen peroxide for 10 min. Target retrieval was performed with RNAscope target retrieval reagents at 99°C for 5 min. The sections were then pretreated with Protease III (RNAScope) for 40 min at 40°C. RNAscope probes (Advanced Cell Diagnostics) for mCherry (Cat No. 431201-C3) and vGAT (Cat No. 424541) were hybridized at 40°C for 2h, serially amplified, and revealed with horseradish peroxidase, Opal Dye/TSA Plus fluorophore (Akoya Biosciences), and horseradish peroxidase blocker. Sections were cover-slipped with anti-fading mounting medium with DAPI (Vectashield, Vectorlabs) and kept in the refrigerator. Images were generated by using an epifluorescent microscope (Nikon, Eclipse NiE Fully Motorized

Upright Microscope) equipped with a fluorescent lamp (X-Cite, 120 LED) and a digital camera (Andor Zyla 4.2 PLUS sCMOS). Expression of mCherry mRNA (red, Opal 620) and GAD67 mRNA (green, Opal 520) was determined by using an automated fluorescent threshold detector (NIS-Elements). Colabeled cells were manually counted by an experimenter by measuring either the percentage of mCherry positive neurons in PL that were also labeled with GAD67, or the percentage of GAD67 positive neurons in PL that were also labeled with mCherry.

Data analyses

Behavioral quantification and statistical analysis. Rats were recorded with digital video cameras (Logitech C920) and behavioral responses were measured by using an automated video-tracking system (ANY-maze) or machine learning (DeepLabCut). Presses per minute were calculated by measuring the number of presses during the 30 s cue multiplied by two. All graphics and numerical values reported in the figures are presented as mean ± s.e.m. Statistical significance was determined with paired or unpaired Student's t test, repeated-measures ANOVA followed by Bonferroni post-hoc comparisons (Prism 7), and Z-test or Fisher's exact test, as indicated in Table 1S. Sample size was based on estimations by power analysis with a level of significance of 0.05 and a power of 0.9.

Single-unit analyses. Based on data from NeuroExplorer, waveform data and spike timestamps for firing rates was processed through Matlab scripting. The principal-component scores for unsorted waveforms were computed and plotted in a three (or two) dimensional principal-component space. Clusters containing similar valid waveforms were manually defined. After manually clustering similar valid waveforms, a

group of spikes were considered from a single neuron if the waveforms formed a discrete, isolated, cluster in the principal-component space. The separation of putative PL^{GLUT} neurons and putative PL^{GABA} neurons was made through an unbiased unsupervised cluster-separation algorithm based on two electrophysiological properties: neuron's average half-spike width (ms) and firing rate (Hz) (Frank et al., 2001). Only *in vivo* photoidentified PL neurons (i.e., GABAergic or glutamatergic) were considered for these analyses. To separate putative PL^{GLUT} neurons and putative PL^{GABA} we used an unsupervised cluster algorithm based on Matlab's k-means++ algorithm for centroid initialization and squared Euclidean distance (Arthur and Vassilvitskii, 2007). The Euclidian distance was calculated between all neuron pairs to detect 2 clusters on the two-dimensional space defined by each cluster representing putative GABAergic or glutamatergic neurons.

Data availability

All the data that support the findings presented in this study are available from the corresponding author on reasonable request.

988 **REFERENCES**

989

990 Ainslie G (1975) Specious reward: a behavioral theory of impulsiveness and impulse
991 control. Psychol Bull 82:463-496.
992 Amir A, Lee SC, Headley DB, Herzallah MM, Pare D (2015) Amygdala Signaling during
993 Foraging in a Hazardous Environment. J Neurosci 35:12994-13005.
994 Arthur D, Vassilvitskii S (2007) K-means++: The Advantages of Careful Seeding. SODA
995 '07: Proceedings of the Eighteenth Annual ACM-SIAM Symposium on Discrete
996 Algorithms:1027-1035.
997 Aupperle RL, Paulus MP (2010) Neural systems underlying approach and avoidance in
998 anxiety disorders. Dialogues Clin Neurosci 12:517-531.
999 Baeg EH, Kim YB, Jang J, Kim HT, Mook-Jung I, Jung MW (2001) Fast spiking and
1000 regular spiking neural correlates of fear conditioning in the medial prefrontal
1001 cortex of the rat. Cereb Cortex 11:441-451.
1002 Bari A, Theobald DE, Caprioli D, Mar AC, Aidoo-Micah A, Dalley JW, Robbins TW
1003 (2010) Serotonin modulates sensitivity to reward and negative feedback in a
1004 probabilistic reversal learning task in rats. Neuropsychopharmacology 35:1290-
1005 1301.
1006 Barker TV, Buzzell GA, Fox NA (2019) Approach, avoidance, and the detection of
1007 conflict in the development of behavioral inhibition. New Ideas Psychol 53:2-12.
1008 Bartho P, Hirase H, Monconduit L, Zugaro M, Harris KD, Buzsaki G (2004)
1009 Characterization of neocortical principal cells and interneurons by network
1010 interactions and extracellular features. J Neurophysiol 92:600-608.
1011 Becchetti A, Gullo F, Bruno G, Dossi E, Lecchi M, Wanke E (2012) Exact distinction of
1012 excitatory and inhibitory neurons in neural networks: a study with GFP-GAD67
1013 neurons optically and electrophysiologically recognized on multielectrode arrays.
1014 Front Neural Circuits 6:63.
1015 Berglind WJ, See RE, Fuchs RA, Ghee SM, Whitfield TW, Jr., Miller SW, McGinty JF
1016 (2007) A BDNF infusion into the medial prefrontal cortex suppresses cocaine
1017 seeking in rats. Eur J Neurosci 26:757-766.
1018 Beyeler A, Namburi P, Glober GF, Simonnet C, Calhoon GG, Conyers GF, Luck R,
1019 Wildes CP, Tye KM (2016) Divergent Routing of Positive and Negative
1020 Information from the Amygdala during Memory Retrieval. Neuron 90:348-361.
1021 Blanchard DC, Griebel G, Pobbe R, Blanchard RJ (2011) Risk assessment as an
1022 evolved threat detection and analysis process. Neurosci Biobehav Rev 35:991-
1023 998.
1024 Bravo-Rivera H, Rubio Arzola P, Caban-Murillo A, Velez-Aviles AN, Ayala-Rosario SN,
1025 Quirk GJ (2021) Characterizing Different Strategies for Resolving Approach-
1026 Avoidance Conflict. Front Neurosci 15:608922.
1027 Breton JM, Charbit AR, Snyder BJ, Fong PTK, Dias EV, Himmels P, Lock H, Margolis
1028 EB (2019) Relative contributions and mapping of ventral tegmental area
1029 dopamine and GABA neurons by projection target in the rat. J Comp Neurol
1030 527:916-941.

Burgos-Robles A, Vidal-Gonzalez I, Quirk GJ (2009) Sustained conditioned responses in prelimbic prefrontal neurons are correlated with fear expression and extinction failure. J Neurosci 29:8474-8482.

Burgos-Robles A, Bravo-Rivera H, Quirk GJ (2013) Prelimbic and infralimbic neurons signal distinct aspects of appetitive instrumental behavior. PLoS One 8:e57575.

Burgos-Robles A, Kimchi EY, Izadmehr EM, Porzenheim MJ, Ramos-Guasp WA, Nieh EH, Felix-Ortiz AC, Namburi P, Leppla CA, Presbrey KN, Anandalingam KK, Pagan-Rivera PA, Anahtar M, Beyeler A, Tye KM (2017) Amygdala inputs to prefrontal cortex guide behavior amid conflicting cues of reward and punishment. Nat Neurosci.

Cain CK (2019) Avoidance Problems Reconsidered. Curr Opin Behav Sci 26:9-17.

Capuzzo G, Floresco SB (2020) Prelimbic and Infralimbic Prefrontal Regulation of Active and Inhibitory Avoidance and Reward-Seeking. J Neurosci 40:4773-4787.

Chen BT, Yau HJ, Hatch C, Kusumoto-Yoshida I, Cho SL, Hopf FW, Bonci A (2013) Rescuing cocaine-induced prefrontal cortex hypoactivity prevents compulsive cocaine seeking. Nature 496:359-362.

Choi EA, McNally GP (2017) Paraventricular Thalamus Balances Danger and Reward. J Neurosci 37:3018-3029.

Choi EA, Jean-Richard-Dit-Bressel P, Clifford CWG, McNally GP (2019) Paraventricular Thalamus Controls Behavior during Motivational Conflict. J Neurosci 39:4945-4958.

Cohen JY, Haesler S, Vong L, Lowell BB, Uchida N (2012) Neuron-type-specific signals for reward and punishment in the ventral tegmental area. Nature 482:85-88.

Constantinidis C, Goldman-Rakic PS (2002) Correlated discharges among putative pyramidal neurons and interneurons in the primate prefrontal cortex. J Neurophysiol 88:3487-3497.

Courtin J, Chaudun F, Rozeske RR, Karalis N, Gonzalez-Campo C, Wurtz H, Abdi A, Baufreton J, Bienvenu TC, Herry C (2014) Prefrontal parvalbumin interneurons shape neuronal activity to drive fear expression. Nature 505:92-96.

Cummings KA, Clem RL (2020) Prefrontal somatostatin interneurons encode fear memory. Nat Neurosci 23:61-74.

Dejean C, Courtin J, Karalis N, Chaudun F, Wurtz H, Bienvenu TC, Herry C (2016) Prefrontal neuronal assemblies temporally control fear behaviour. Nature 535:420-424.

Dellu-Hagedorn F, Rivalan M, Fitoussi A, De Deurwaerdere P (2018) Inter-individual differences in the impulsive/compulsive dimension: deciphering related dopaminergic and serotonergic metabolisms at rest. Philos Trans R Soc Lond B Biol Sci 373.

Diehl MM, Bravo-Rivera C, Rodriguez-Romaguera J, Pagan-Rivera PA, Burgos-Robles A, Roman-Ortiz C, Quirk GJ (2018) Active avoidance requires inhibitory signaling in the rodent prelimbic prefrontal cortex. Elife 7.

Dimidschstein J et al. (2016) A viral strategy for targeting and manipulating interneurons across vertebrate species. Nat Neurosci 19:1743-1749.

Do-Monte FH, Quinones-Laracuente K, Quirk GJ (2015) A temporal shift in the circuits mediating retrieval of fear memory. Nature 519:460-463.

Do-Monte FH, Rodriguez-Romaguera J, Rosas-Vidal LE, Quirk GJ (2013) Deep brain stimulation of the ventral striatum increases BDNF in the fear extinction circuit. Front Behav Neurosci 7:102.

Do Monte FH, Quirk GJ, Li B, Penzo MA (2016) Retrieving fear memories, as time goes by. Mol Psychiatry 21:1027-1036.

Emmons EB, Ruggiero RN, Kelley RM, Parker KL, Narayanan NS (2016) Corticostriatal Field Potentials Are Modulated at Delta and Theta Frequencies during Interval-Timing Task in Rodents. Front Psychol 7:459.

Engelke DS, Zhang XO, O'Malley JJ, Fernandez-Leon JA, Li S, Kirouac GJ, Beierlein M, Do-Monte FH (2021) A hypothalamic-thalamostriatal circuit that controls approach-avoidance conflict in rats. Nat Commun 12:2517.

Fan H, Pan X, Wang R, Sakagami M (2017) Differences in reward processing between putative cell types in primate prefrontal cortex. PLoS One 12:e0189771.

Ferenczi EA, Zalocusky KA, Liston C, Grosenick L, Warden MR, Amatya D, Katovich K, Mehta H, Patenaude B, Ramakrishnan C, Kalanithi P, Etkin A, Knutson B, Glover GH, Deisseroth K (2016) Prefrontal cortical regulation of brainwide circuit dynamics and reward-related behavior. Science 351:aac9698.

Flagel SB, Watson SJ, Robinson TE, Akil H (2007) Individual differences in the propensity to approach signals vs goals promote different adaptations in the dopamine system of rats. Psychopharmacology (Berl) 191:599-607.

Flagel SB, Clark JJ, Robinson TE, Mayo L, Czuj A, Willuhn I, Akers CA, Clinton SM, Phillips PE, Akil H (2011) A selective role for dopamine in stimulus-reward learning. Nature 469:53-57.

Frank LM, Brown EN, Wilson MA (2001) A comparison of the firing properties of putative excitatory and inhibitory neurons from CA1 and the entorhinal cortex. J Neurophysiol 86:2029-2040.

Gabbott PL, Warner TA, Jays PR, Salway P, Busby SJ (2005) Prefrontal cortex in the rat: projections to subcortical autonomic, motor, and limbic centers. J Comp Neurol 492:145-177.

Gaykema RP, Nguyen XM, Boehret JM, Lambeth PS, Joy-Gaba J, Warthen DM, Scott MM (2014) Characterization of excitatory and inhibitory neuron activation in the mouse medial prefrontal cortex following palatable food ingestion and food driven exploratory behavior. Front Neuroanat 8:60.

Geller I (1960) The acquisition and extinction of conditioned suppression as a function of the base-line reinforcer. J Exp Anal Behav 3:235-240.

Gradinaru V, Mogri M, Thompson KR, Henderson JM, Deisseroth K (2009) Optical deconstruction of parkinsonian neural circuitry. Science 324:354-359.

Haight JL, Fuller ZL, Fraser KM, Flagel SB (2017) A food-predictive cue attributed with incentive salience engages subcortical afferents and efferents of the paraventricular nucleus of the thalamus. Neuroscience 340:135-152.

Harris AZ, Gordon JA (2015) Long-range neural synchrony in behavior. Annu Rev Neurosci 38:171-194.

Hassani OK, Lee MG, Henny P, Jones BE (2009) Discharge profiles of identified GABAergic in comparison to cholinergic and putative glutamatergic basal forebrain neurons across the sleep-wake cycle. J Neurosci 29:11828-11840.

Horst NK, Laubach M (2013) Reward-related activity in the medial prefrontal cortex is driven by consumption. Front Neurosci 7:56.

Hu H (2016) Reward and Aversion. Annu Rev Neurosci 39:297-324.

Hyman JM, Hasselmo ME, Seamans JK (2011) What is the Functional Relevance of Prefrontal Cortex Entrainment to Hippocampal Theta Rhythms? Front Neurosci 5:24.

Jean-Richard-Dit-Bressel P, Ma C, Bradfield LA, Killcross S, McNally GP (2019) Punishment insensitivity emerges from impaired contingency detection, not aversion insensitivity or reward dominance. Elife 8.

Jensen J, Walter H (2014) Incentive motivational salience and the human brain. Restor Neurol Neurosci 32:141-147.

Karalis N, Dejean C, Chaudun F, Khoder S, Rozeske RR, Wurtz H, Bagur S, Benchenane K, Sirota A, Courtin J, Herry C (2016) 4-Hz oscillations synchronize prefrontal-amygdala circuits during fear behavior. Nat Neurosci.

Kim CK, Ye L, Jennings JH, Pichamoorthy N, Tang DD, Yoo AW, Ramakrishnan C, Deisseroth K (2017) Molecular and Circuit-Dynamical Identification of Top-Down Neural Mechanisms for Restraint of Reward Seeking. Cell 170:1013-1027 e1014.

Kim EJ, Kim N, Kim HT, Choi JS (2013) The prelimbic cortex is critical for context-dependent fear expression. Front Behav Neurosci 7:73.

Kim EJ, Kong MS, Park SG, Mizumori SJY, Cho J, Kim JJ (2018) Dynamic coding of predatory information between the prelimbic cortex and lateral amygdala in foraging rats. Sci Adv 4:eaar7328.

Kirlic N, Young J, Aupperle RL (2017) Animal to human translational paradigms relevant for approach avoidance conflict decision making. Behav Res Ther 96:14-29.

Kroener S, Chandler LJ, Phillips PE, Seamans JK (2009) Dopamine modulates persistent synaptic activity and enhances the signal-to-noise ratio in the prefrontal cortex. PLoS One 4:e6507.

Krypotos AM, Effting M, Kindt M, Beckers T (2015) Avoidance learning: a review of theoretical models and recent developments. Front Behav Neurosci 9:189.

Kyriazi P, Headley DB, Pare D (2020) Different Multidimensional Representations across the Amygdalo-Prefrontal Network during an Approach-Avoidance Task. Neuron 107:717-730 e715.

Likhtik E, Paz R (2015) Amygdala-prefrontal interactions in (mal)adaptive learning. Trends Neurosci 38:158-166.

Likhtik E, Stujenske JM, Topiwala MA, Harris AZ, Gordon JA (2014) Prefrontal entrainment of amygdala activity signals safety in learned fear and innate anxiety. Nat Neurosci 17:106-113.

Lima SQ, Hromadka T, Znamenskiy P, Zador AM (2009) PINP: a new method of tagging neuronal populations for identification during in vivo electrophysiological recording. PLoS One 4:e6099.

Marquis JP, Killcross S, Haddon JE (2007) Inactivation of the prelimbic, but not infralimbic, prefrontal cortex impairs the contextual control of response conflict in rats. Eur J Neurosci 25:559-566.

Mathis A, Mamidanna P, Cury KM, Abe T, Murthy VN, Mathis MW, Bethge M (2018) DeepLabCut: markerless pose estimation of user-defined body parts with deep learning. Nat Neurosci 21:1281-1289.

McDonald AJ (1991) Organization of amygdaloid projections to the prefrontal cortex and associated striatum in the rat. Neuroscience 44:1-14.

McGinley MJ, David SV, McCormick DA (2015) Cortical Membrane Potential Signature of Optimal States for Sensory Signal Detection. Neuron 87:179-192.

McGinty JF, Otis JM (2020) Heterogeneity in the Paraventricular Thalamus: The Traffic Light of Motivated Behaviors. Front Behav Neurosci 14:590528.

McNaughton N, Corr PJ (2014) Approach, avoidance, and their conflict: the problem of anchoring. Front Syst Neurosci 8:124.

Millan EZ, Ong Z, McNally GP (2017) Paraventricular thalamus: Gateway to feeding, appetitive motivation, and drug addiction. Prog Brain Res 235:113-137.

Moorman DE, Aston-Jones G (2015) Prefrontal neurons encode context-based response execution and inhibition in reward seeking and extinction. Proc Natl Acad Sci U S A 112:9472-9477.

Morales I, Berridge KC (2020) 'Liking' and 'wanting' in eating and food reward: Brain mechanisms and clinical implications. Physiol Behav 227:113152.

Mruczek RE, Sheinberg DL (2012) Stimulus selectivity and response latency in putative inhibitory and excitatory neurons of the primate inferior temporal cortex. J Neurophysiol 108:2725-2736.

Nair-Roberts RG, Chatelain-Badie SD, Benson E, White-Cooper H, Bolam JP, Ungless MA (2008) Stereological estimates of dopaminergic, GABAergic and glutamatergic neurons in the ventral tegmental area, substantia nigra and retrorubral field in the rat. Neuroscience 152:1024-1031.

Namburi P, Beyeler A, Yorozu S, Calhoon GG, Halbert SA, Wichmann R, Holden SS, Mertens KL, Anahtar M, Felix-Ortiz AC, Wickersham IR, Gray JM, Tye KM (2015) A circuit mechanism for differentiating positive and negative associations. Nature 520:675-678.

Narayanan NS, Cavanagh JF, Frank MJ, Laubach M (2013) Common medial frontal mechanisms of adaptive control in humans and rodents. Nat Neurosci 16:1888-1895.

Oberrauch S, Sigrist H, Sautter E, Gerster S, Bach DR, Pryce CR (2019) Establishing operant conflict tests for the translational study of anxiety in mice. Psychopharmacology (Berl) 236:2527-2541.

Ono M, Bishop DC, Oliver DL (2017) Identified GABAergic and Glutamatergic Neurons in the Mouse Inferior Colliculus Share Similar Response Properties. J Neurosci 37:8952-8964.

Orsini CA, Heshmati SC, Garman TS, Wall SC, Bizon JL, Setlow B (2018) Contributions of medial prefrontal cortex to decision making involving risk of punishment. Neuropharmacology 139:205-216.

Otis JM, Namboodiri VM, Matan AM, Voets ES, Mohorn EP, Kosyk O, McHenry JA, Robinson JE, Resendez SL, Rossi MA, Stuber GD (2017) Prefrontal cortex output circuits guide reward seeking through divergent cue encoding. Nature 543:103-107.

Padilla-Coreano N, Canetta S, Mikofsky RM, Alway E, Passecker J, Myroshnychenko MV, Garcia-Garcia AL, Warren R, Teboul E, Blackman DR, Morton MP, Hupalo S, Tye KM, Kellendonk C, Kupferschmidt DA, Gordon JA (2019) Hippocampal-

Prefrontal Theta Transmission Regulates Avoidance Behavior. Neuron 104:601-610 e604.

Park J, Moghaddam B (2017) Risk of punishment influences discrete and coordinated encoding of reward-guided actions by prefrontal cortex and VTA neurons. Elife 6.

Penzo MA, Gao C (2021) The paraventricular nucleus of the thalamus: an integrative node underlying homeostatic behavior. Trends Neurosci.

Pi HJ, Hangya B, Kvitsiani D, Sanders JI, Huang ZJ, Kepecs A (2013) Cortical interneurons that specialize in disinhibitory control. Nature 503:521-524.

Piantadosi PT, Yeates DCM, Floresco SB (2020) Prefrontal cortical and nucleus accumbens contributions to discriminative conditioned suppression of reward-seeking. Learn Mem 27:429-440.

Popa D, Duvarci S, Popescu AT, Lena C, Pare D (2010) Coherent amygdalocortical theta promotes fear memory consolidation during paradoxical sleep. Proc Natl Acad Sci U S A 107:6516-6519.

Radke AK, Nakazawa K, Holmes A (2015) Cortical GluN2B deletion attenuates punished suppression of food reward-seeking. Psychopharmacology (Berl) 232:3753-3761.

Robinson TE, Flagel SB (2009) Dissociating the predictive and incentive motivational properties of reward-related cues through the study of individual differences. Biol Psychiatry 65:869-873.

Robinson TE, Yager LM, Cogan ES, Saunders BT (2014) On the motivational properties of reward cues: Individual differences. Neuropharmacology 76 Pt B:450-459.

Sangha S, Robinson PD, Greba Q, Davies DA, Howland JG (2014) Alterations in reward, fear and safety cue discrimination after inactivation of the rat prelimbic and infralimbic cortices. Neuropsychopharmacology 39:2405-2413.

Santana N, Bortolozzi A, Serrats J, Mengod G, Artigas F (2004) Expression of serotonin1A and serotonin2A receptors in pyramidal and GABAergic neurons of the rat prefrontal cortex. Cereb Cortex 14:1100-1109.

Schultz W (2015) Neuronal Reward and Decision Signals: From Theories to Data. Physiol Rev 95:853-951.

Serrano-Barroso A, Vargas JP, Diaz E, O'Donnell P, Lopez JC (2019) Sign and goal tracker rats process differently the incentive salience of a conditioned stimulus. PLoS One 14:e0223109.

Sharpe MJ, Killcross S (2015) The prelimbic cortex directs attention toward predictive cues during fear learning. Learn Mem 22:289-293.

Sierra-Mercado D, Padilla-Coreano N, Quirk GJ (2011) Dissociable roles of prelimbic and infralimbic cortices, ventral hippocampus, and basolateral amygdala in the expression and extinction of conditioned fear. Neuropsychopharmacology 36:529-538.

Simon NW, Gilbert RJ, Mayse JD, Bizon JL, Setlow B (2009) Balancing risk and reward: a rat model of risky decision making. Neuropsychopharmacology 34:2208-2217.

Smith KS, Berridge KC, Aldridge JW (2011) Disentangling pleasure from incentive salience and learning signals in brain reward circuitry. Proc Natl Acad Sci U S A 108:E255-264.

Sotres-Bayon F, Sierra-Mercado D, Pardilla-Delgado E, Quirk GJ (2012) Gating of fear in prelimbic cortex by hippocampal and amygdala inputs. Neuron 76:804-812.

St Onge JR, Floresco SB (2009) Dopaminergic modulation of risk-based decision making. Neuropsychopharmacology 34:681-697.

Stujenske JM, Likhtik E, Topiwala MA, Gordon JA (2014) Fear and safety engage competing patterns of theta-gamma coupling in the basolateral amygdala. Neuron 83:919-933.

Sun X, Bernstein MJ, Meng M, Rao S, Sorensen AT, Yao L, Zhang X, Anikeeva PO, Lin Y (2020) Functionally Distinct Neuronal Ensembles within the Memory Engram. Cell 181:410-423 e417.

Tan KR, Yvon C, Turiault M, Mirzabekov JJ, Doehner J, Labouebe G, Deisseroth K, Tye KM, Luscher C (2012) GABA neurons of the VTA drive conditioned place aversion. Neuron 73:1173-1183.

Tomie A, Aguado AS, Pohorecky LA, Benjamin D (2000) Individual differences in pavlovian autoshaping of lever pressing in rats predict stress-induced corticosterone release and mesolimbic levels of monoamines. Pharmacol Biochem Behav 65:509-517.

Totah NK, Jackson ME, Moghaddam B (2013) Preparatory attention relies on dynamic interactions between prelimbic cortex and anterior cingulate cortex. Cereb Cortex 23:729-738.

Treanor M, Barry TJ (2017) Treatment of avoidance behavior as an adjunct to exposure therapy: Insights from modern learning theory. Behav Res Ther 96:30-36.

Tye KM, Prakash R, Kim SY, Fenno LE, Grosenick L, Zarabi H, Thompson KR, Gradinaru V, Ramakrishnan C, Deisseroth K (2011) Amygdala circuitry mediating reversible and bidirectional control of anxiety. Nature 471:358-362.

van Zessen R, Phillips JL, Budygin EA, Stuber GD (2012) Activation of VTA GABA neurons disrupts reward consumption. Neuron 73:1184-1194.

Verharen JPH, van den Heuvel MW, Luijendijk M, Vanderschuren L, Adan RAH (2019) Corticolimbic Mechanisms of Behavioral Inhibition under Threat of Punishment. J Neurosci 39:4353-4364.

Vertes RP (2004) Differential projections of the infralimbic and prelimbic cortex in the rat. Synapse 51:32-58.

Vidal-Gonzalez I, Vidal-Gonzalez B, Rauch SL, Quirk GJ (2006) Microstimulation reveals opposing influences of prelimbic and infralimbic cortex on the expression of conditioned fear. Learn Mem 13:728-733.

Vigneswaran G, Kraskov A, Lemon RN (2011) Large identified pyramidal cells in macaque motor and premotor cortex exhibit "thin spikes": implications for cell type classification. J Neurosci 31:14235-14242.

Vogel JR, Beer B, Clody DE (1971) A simple and reliable conflict procedure for testing anti-anxiety agents. Psychopharmacologia 21:1-7.

Volkow ND, Wang GJ, Fowler JS, Tomasi D, Baler R (2012) Food and drug reward: overlapping circuits in human obesity and addiction. Curr Top Behav Neurosci 11:1-24.

Wakabayashi KT, Feja M, Baindur AN, Bruno MJ, Bhimani RV, Park J, Hausknecht K, Shen RY, Haj-Dahmane S, Bass CE (2019) Chemogenetic activation of ventral tegmental area GABA neurons, but not mesoaccumbal GABA terminals, disrupts responding to reward-predictive cues. Neuropsychopharmacology 44:372-380.

Warthen DM, Lambeth PS, Ottolini M, Shi Y, Barker BS, Gaykema RP, Newmyer BA, Joy-Gaba J, Ohmura Y, Perez-Reyes E, Guler AD, Patel MK, Scott MM (2016) Activation of Pyramidal Neurons in Mouse Medial Prefrontal Cortex Enhances Food-Seeking Behavior While Reducing Impulsivity in the Absence of an Effect on Food Intake. Front Behav Neurosci 10:63.

Weir K, Blanquie O, Kilb W, Luhmann HJ, Sinning A (2014) Comparison of spike parameters from optically identified GABAergic and glutamatergic neurons in sparse cortical cultures. Front Cell Neurosci 8:460.

Widge AS, Heilbronner SR, Hayden BY (2019) Prefrontal cortex and cognitive control: new insights from human electrophysiology. F1000Res 8.

Zhang X, Kim J, Tonegawa S (2020) Amygdala Reward Neurons Form and Store Fear Extinction Memory. Neuron 105:1077-1093 e1077.

FIGURE 1

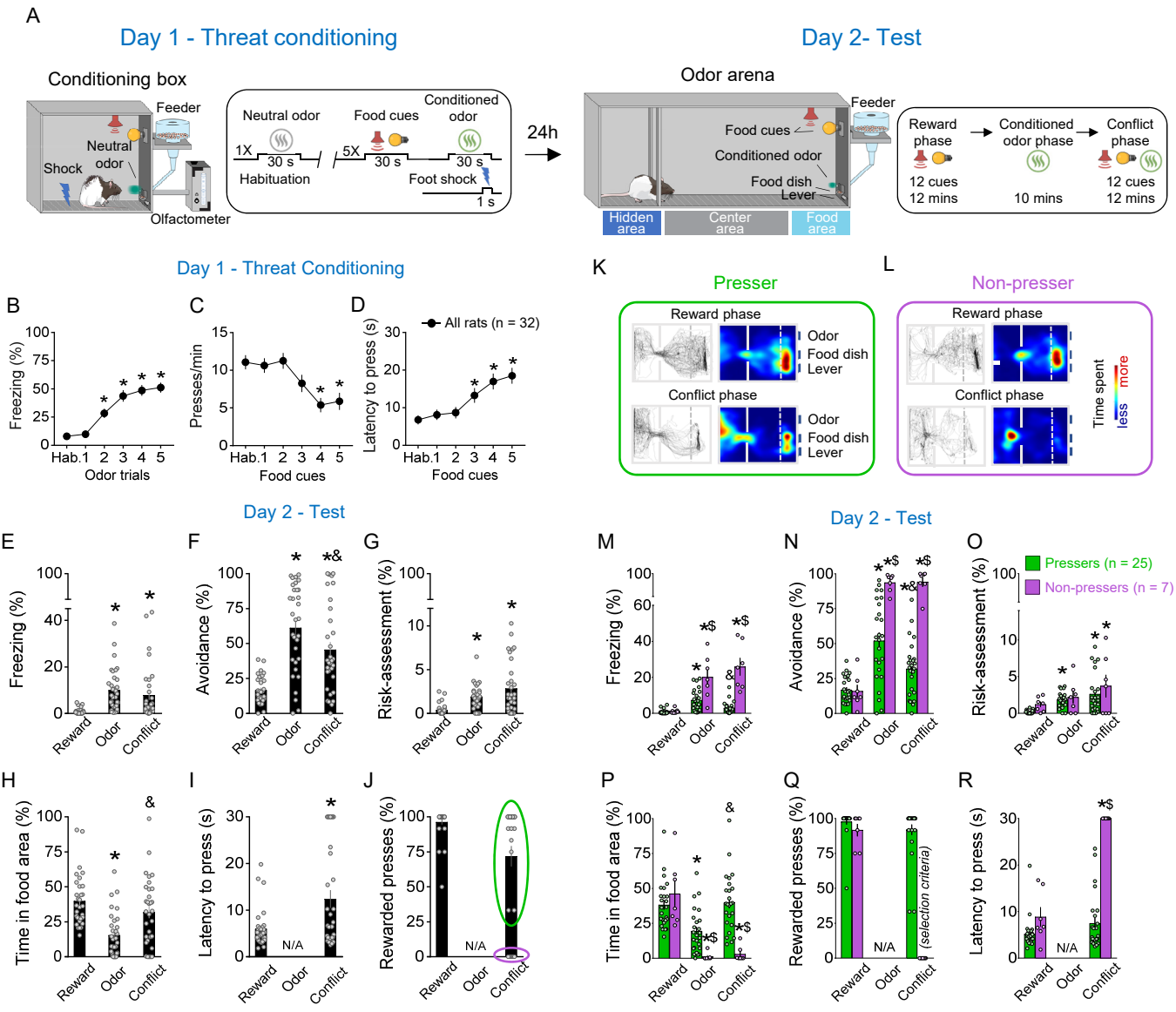

Figure 1. Rats show individual variability in reward-seeking responses during an approach-avoidance conflict test. (A) Schematic and timeline of the approach-avoidance conflict test. **(B-D)** Rats exhibited an increase in the percentage of time freezing ($F_{(3.117, 96.63)} = 30.4$, $p < 0.0001$) and a reduction in lever presses ($F_{(3.771, 116.9)} = 11.59$, $p < 0.0001$) with a higher latency to press the lever ($F_{(3.29, 102)} = 13.09$, $p < 0.0001$) during the olfactory threat conditioning session on day 1 (n = 32), when compared to before the shock. **(E-G)** Patterns of defensive responses and food seeking during the different phases (reward, odor, conflict) of the test session on day 2. Rats showed an increase in defensive responses characterized by an augment in the percentage of time exhibiting (E) freezing ($F_{(1.678, 52.01)} = 16.56$, $p < 0.0001$), (F) avoidance ($F_{(1.85, 57.36)} = 38.99$, $p < 0.0001$) and (G) risk-assessment ($F_{(1.367, 42.38)} = 17.41$, $p = 0.014$) ; and a decrease in the (H) percentage of time spent in the food area ($F_{(1.63, 50.52)} = 23.81$, $p < 0.0001$) during the odor presentation, when compared to the reward phase. Rats' defensive responses were significantly attenuated during the conflict phase as evidenced by a reduction in the percentage of time (F) avoiding the odor ($p = 0.0031$) and an increase in the percentage of time (H) approaching the food area ($p < 0.0001$) , when compared to the odor phase. **(I-J)** Two different behavioral phenotypes emerged during the conflict phase: rats that continued to press the lever (*Pressers*, green circle, n= 25) and rats that showed a complete suppression in lever pressing (*Non-pressers*, purple circle, n= 7). The % of rewarded presses was calculated as the percentage of the 12 cue trials in which rats pressed the lever. **(K-L)** Representative tracks and heatmaps of time spent in each compartment of the arena for a (K) *Presser* or a (L) Non-Pressers rat during the test session. **(M-R)** Patterns of defensive responses and food seeking during the different phases (reward, odor, conflict) of the test session on day 2 after separating the animals into *Pressers* and *Non-pressers.* When compared to *Non-Pressers, Pressers* showed reduced defensive responses characterized by an attenuation in the percentage of time exhibiting (M) freezing ($F_{(2, 60)} = 29.54$, $p < 0.0001$) and (N) avoidance responses ($F_{(2, 60)} = 23.27$, $p < 0.0001$), and an augment in the percentage of time (P) approaching the food area ($F_{(2, 60)} = 22.49$, $p<0.0001$) during both the odor and the conflict phases. Data shown as mean ± SEM. One-way or two-way ANOVA repeated measures followed by Tukey's or Bonferroni's multiple comparisons tests, all * p's < 0.05 compared to the same group during the reward phase, all & p's < 0.05 compared to the same group during the odor phase, all $ p's < 0.05 compared to *Pressers* during the same phase. All statistical analysis details are presented in table S1. See also Supplementary Fig. 1 and Supplementary Video 1.

FIGURE 2

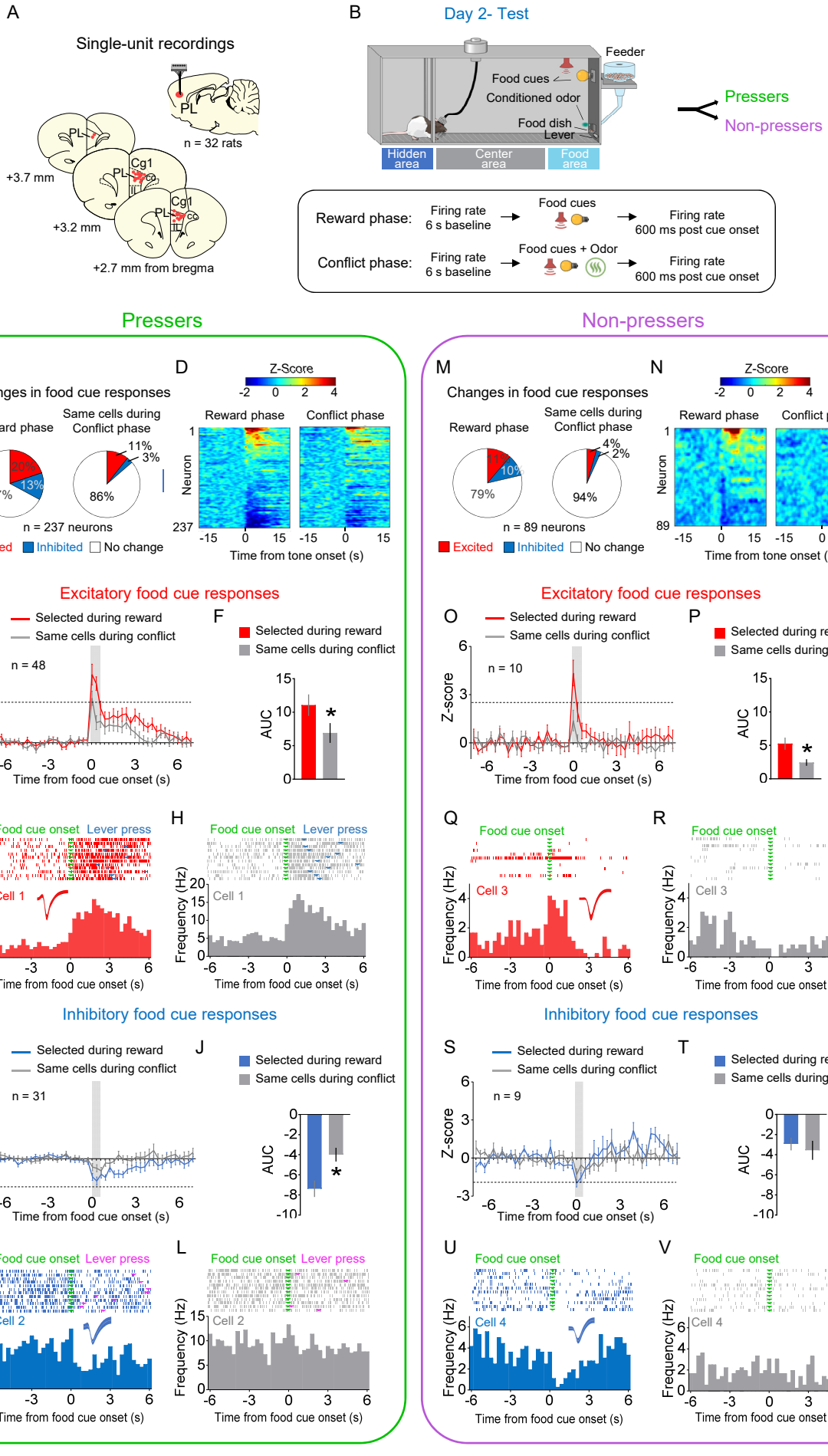

Figure 2. PL neurons respond differently to reward cues in *Pressers* vs. *Non-Pressers* during conflict (A) Diagram of the electrode placements in PL. **B)** Schematic and timeline of PL recordings for food cue responses during of the approach-avoidance conflict test (12 food cues per phase). **(C)** Pie charts showing changes in PL firing rate in response to food cues during reward (left) vs. conflict (right) phases for *Pressers* (n = 237 neurons from 25 rats, Fisher's exact test, excitatory during reward phase: n = 48, excitatory during conflict phase: n = 25, p = 0.0049; inhibitory during reward phase: n = 31, inhibitory during conflict phase: n = 7, p < 0.0001. **(D)** Heatmap of Z-scored neural activities for PL neurons selected during reward phase and tracked to conflict phase. **(E)** Average peri-stimulus time histograms (PSTHs) for all PL neurons showing excitatory food cue responses (Z-score > 2.58, dotted line) during reward (red line) compared to the same cells during conflict (gray line). **(F)** Differences in the positive area under the curve (AUC) between the two phases (Wilcoxon test, W = -824, excitatory responses reward phase vs. conflict phase, p < 0.0001). **(G-H)** Representative PSTHs for a PL neuron showing excitatory responses to food cues during the (G) reward phase vs. the same neuron during the (H) conflict phase. **(I)** Average PSTHs for all PL neurons showing inhibitory food cue responses (Z-score < -1.96, dotted line) during reward (blue line) compared to the same cells during conflict (gray line). **(J)** Differences in the negative AUC between the two phases (Wilcoxon test, W = 367, excitatory responses reward phase vs. conflict phase, p < 0.0001). **(K-L)** Representative PSTHs for a PL neuron showing inhibitory responses to food cues during the reward phase (K) vs. the same neuron during the conflict phase (L). **(M)** Pie charts showing changes in PL firing rate in response to food cues during reward (left) vs. conflict (right) phases for *Non-Pressers* (n= 89 neurons from 7 rats; Fisher's exact test, excitatory during reward phase: n = 10, excitatory during conflict phase: n = 4, p = 0.1620; inhibitory during reward phase: n = 9, inhibitory during conflict phase: n = 2, p = 0.0573). **(N-O)** Same as D-E, but for *Non-Pressers*. **(P)** Differences in the positive AUC between the two phases (Wilcoxon test, W = -37, excitatory responses reward phase vs. conflict phase, p = 0.032). **(Q-S)** Same as G-I, but for *Non-Pressers*. **(T)** Differences in the negative AUC between the two phases (Wilcoxon test, W = -3, excitatory responses reward phase vs. conflict phase, p = 0.455). **(U-V)** Same as K-L, but for *Non-Pressers*. Legend: cc, corpus callosum, CG1, anterior cingulate cortex; IL, infralimbic cortex. All statistical analysis details are presented in table S1. See also Supplementary Figs. 2 and 3.

FIGURE 3

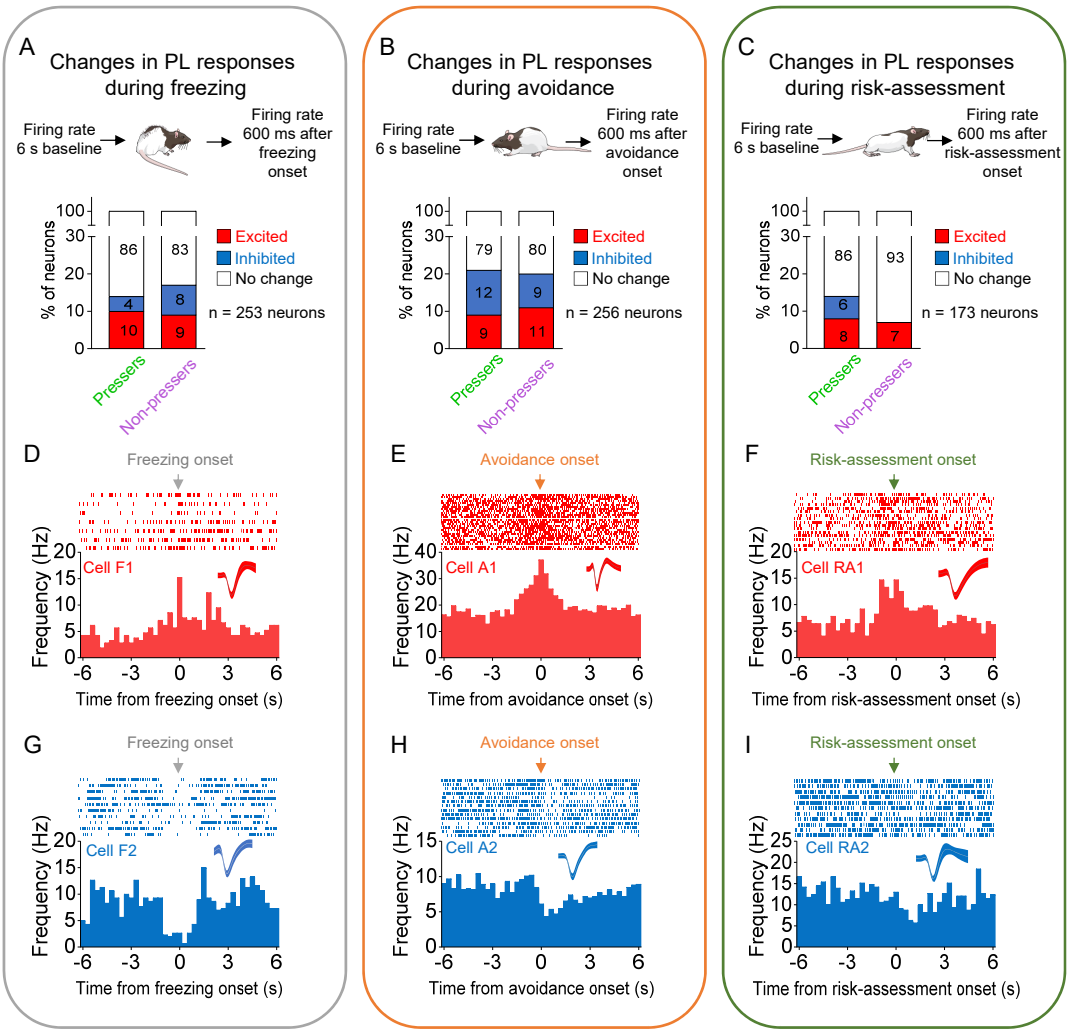

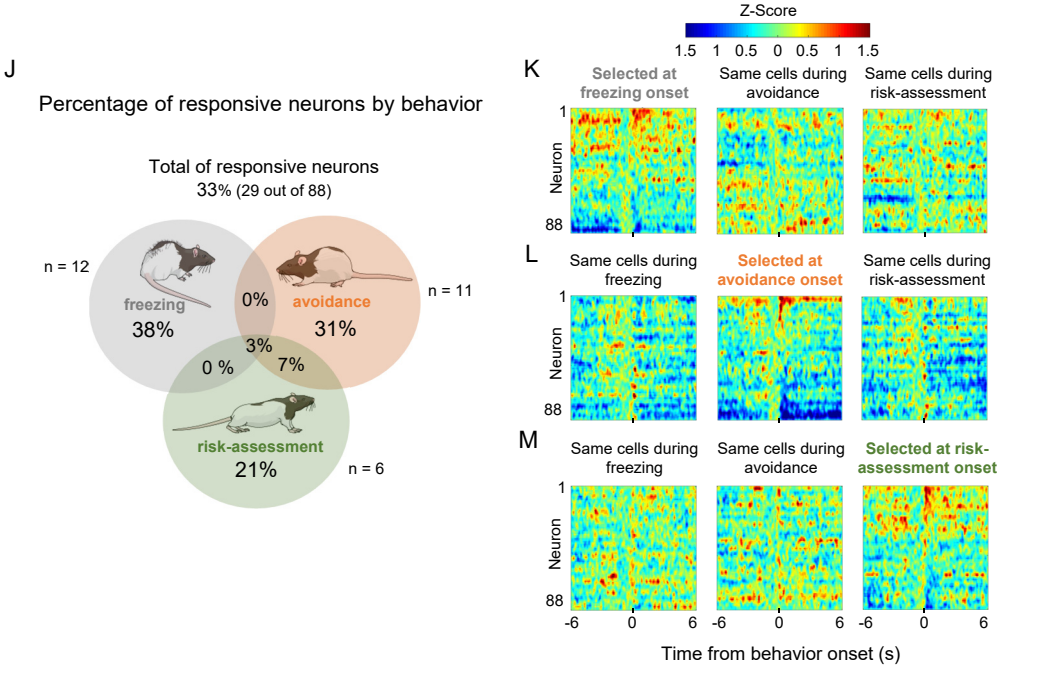

Figure 3. PL activity correlates with the onset of freezing, avoidance or risk-assessment behaviors in both *Pressers* and *Non-Pressers*. (A-C) Both *Pressers* and *Non-Pressers* showed the same number and proportion of excitatory and inhibitory PL responses during the onset of (A) freezing (Fisher's exact test, responsive neurons in *Pressers*: 22 neurons, in *Non-Pressers*: 15 neurons, p = 0.462), (B) avoidance (Fisher's exact test, responsive neurons in *Pressers*: 43 neurons, in *Non-Pressers*: 9 neurons, p = 0.999) or (C) risk-assessment (Fisher's exact test, responsive neurons in *Pressers*: 12 neurons, in *Non-Pressers*: 6 neurons, p = 0.318) behaviors. **(D-F)** Representative PSTHs for distinct PL neurons showing excitatory responses at the onset of (D) freezing, (E) avoidance or (F) risk-assessment behaviors. **(G-I)** Representative PSTHs for distinct PL neurons showing inhibitory responses at the onset of freezing (G), avoidance (H) or risk-assessment (I) behaviors. **(J)** Venn Diagram showing the percentage of all PL responsive neurons (29 out of 88 neurons) by behavior. Most of the responsive neurons responded exclusively at the onset of one of the behaviors. **(K-M)** Heatmap of Z-scored neural activities for PL neurons selected at the onset of freezing (K), avoidance (L) or risk-assessment behavior (M) with the same cells tracked during the other behaviors. The threshold used to identify significant differences per neurons was Z-score > 2.58 for excitation and Z-score < -1.96 for inhibition. All statistical analysis details are presented in table S1.

FIGURE 4

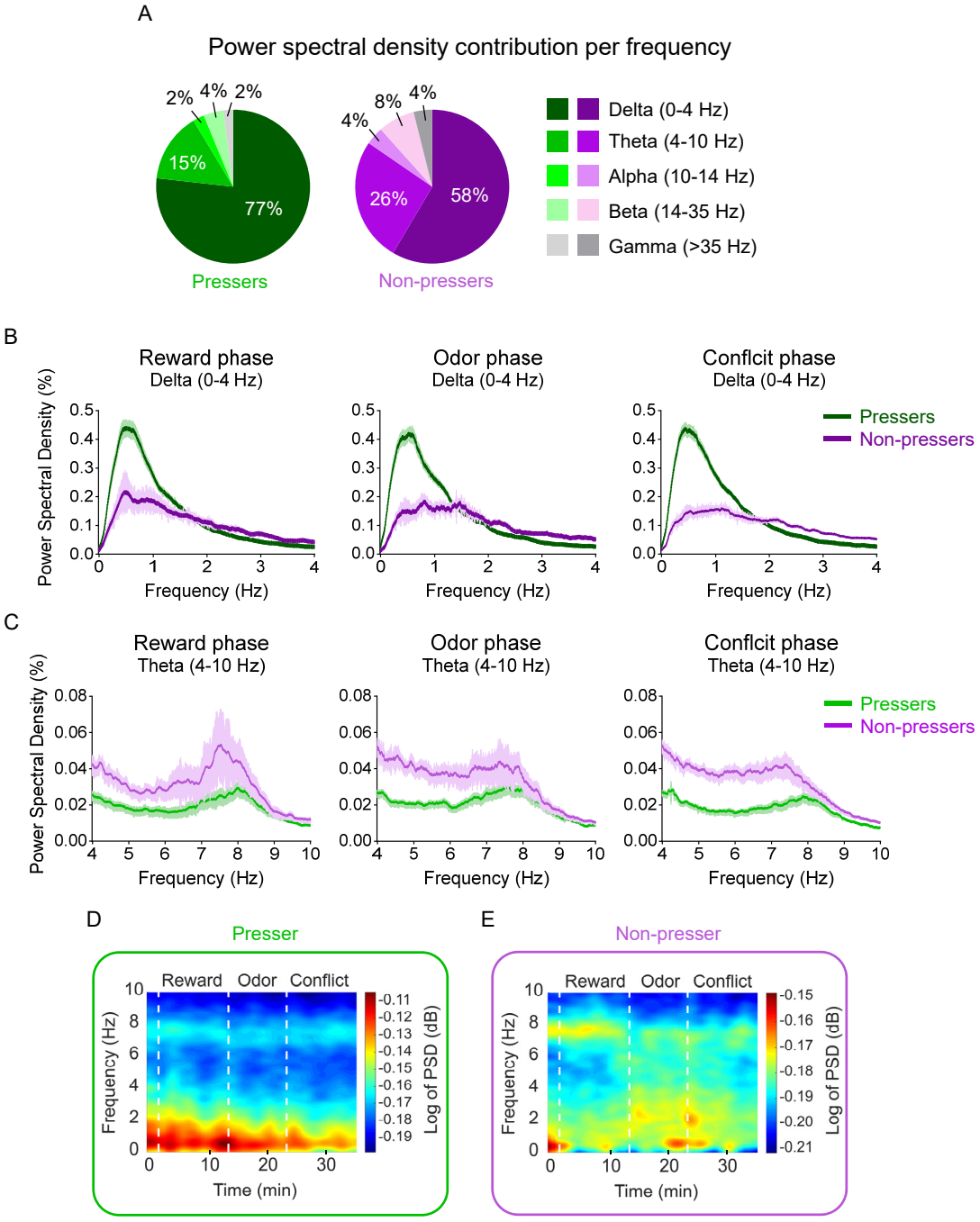

Figure 4. *Pressers* and *Non-Pressers* show significant differences in PL oscillations during the test session. **(A)** Power spectral density (PSD) contribution at different frequency bands. **(B-C)** Average of PSD (%) in the (B) delta (0-4 Hz) or (C) theta (4-10 Hz) bands in *Pressers* (green line, n = 25 rats) and *Non-Pressers* (purple line, n = 7 rats) during the (left) reward, (center) odor, and (right) conflict phases of the test session. *Pressers* showed increased power in the delta band, whereas *Non-Pressers* showed increased power in the theta band during the three phases of the test session (Unpaired Student's t-test comparing *Pressers* vs. *Non-Pressers*, All p's < 0.0001) . **(D-E)** Representative time-frequency spectrogram showing changes in the log of PSD (dB) for delta and theta bands in (D) *Pressers* and (E) *Non-Pressers* across the different phases of the session. All statistical analysis details are presented in table S1.

FIGURE 5

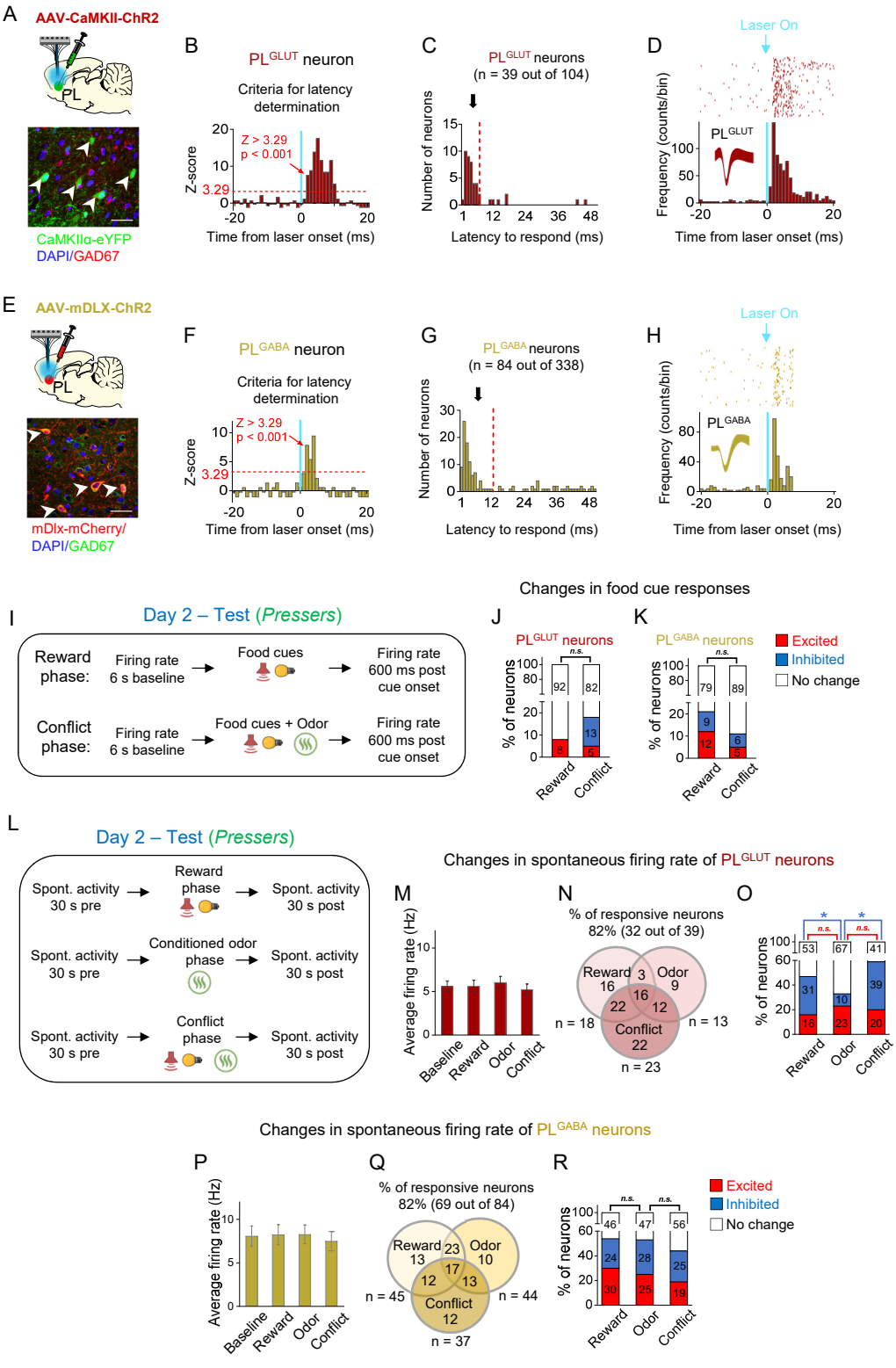

Figure 5. In pressers, PL^{GLUT} neurons show reduced spontaneous activity during the conflict phase. (A) Top, Schematic of viral infusion. Bottom, Representative immunohistochemical micrograph showing lack of colabeling (white arrows) between the ChR2 viral construct (green, AAV-CaMKII-ChR2-eYFP) and the GABA marker GAD67 (red), confirming that the use of a CaMKII promoter enables transgene expression favoring PL glutamatergic neurons. Scale bars: 25 µm. **(B-D)** Photoidentification of PL^{GLUT} neurons. (B) Frequency histogram showing the latency of response to laser illumination for PL neurons (n = 39 photoidentified PL^{GLUT} neurons out of 104 recorded cells). (C) Cells with photoresponse latencies < 6 ms were classified as PL^{GLUT} neurons (Z-score > 3.29, $p < 0.001$, red dotted line, see details in Methods). (D) Raster plot and peristimulus time histogram showing a representative PL^{GLUT} neuron responding to a 5 Hz train of laser stimulation. **(E)** Top, Schematic of viral infusion. Bottom, Representative immunohistochemical micrograph showing colabeling (white arrows) between the ChR2 viral construct (red, AAV-mDlx-ChR2-mCherry) and the GABA marker GAD67 (green), confirming that the use of a mDlx promoter enables transgene expression favoring PL GABA neurons. Scale bars: 25 µm. **(F-H)** Photoidentification of PL^{GABA} neurons. (F) Frequency histogram showing the latency of response to laser illumination for PL neurons (n = 84 photoidentified PL^{GABA} neurons out of 338 recorded neurons). (G) Cells with photoresponse latencies < 12 ms were classified as PL^{GABA} neurons (Z-score > 3.29, $p < 0.001$, red dotted line, see details in Methods). (H) Raster plot and peristimulus time histogram showing a representative PL^{GABA} neuron responding to a 5Hz train of laser stimulation. Vertical blue bars: laser onset. Bins of 1 ms. **(I)** Timeline of PL recordings for food cue responses in *Pressers* during test (12 food cues per phase). **(J-K)** Stacked bar showing the percentage of (J) PL^{GLUT} neurons or (K) PL^{GABA} neurons that changed their firing rates in response to food cues from the reward phase to the conflict phase. No significant differences were observed across the phases (Fisher's exact test, all p's > 0.05; n.s. = non-significant). **(L)** Timeline of PL recordings for spontaneous activity in *Pressers* during test. **(M)** Average firing rate of PL^{GLUT} neurons across the different phases of test. **(N)** Venn diagram showing the percentage of responsive PL^{GLUT} neurons (32 out of 39 neurons) by events. **(O)** Stacked bar showing the percentage of PL^{GLUT} neurons that changed their spontaneous firing rates across the different phases of the test. PL^{GLUT} neurons were disinhibited during the odor phase (Fisher's exact test, inhibited in Reward phase: 12 neurons, inhibited in Odor phase: 4 neurons, $p = 0.047$) and subsequently inhibited during the conflict phase (Fisher's exact test, inhibited in Odor phase: 4 neurons, inhibited in Conflict phase: 15 neurons, $p = 0.0073$). **(P)** Average firing rate of PL^{GABA} neurons across the different phases of test. **(Q)** Venn diagram showing the percentage of responsive PL^{GABA} neurons (69 out of 84 neurons) by events. **(R)** Stacked bar showing the percentage of PL^{GABA} neurons that changed their spontaneous firing rates across the different phases of the test. No significant differences were observed across the phases (Fisher's exact test, all p's > 0.05; n.s. = non-significant). All statistical analysis details are presented in table S1. See also Supplementary Figs. 4, 5, 6 and 7.

FIGURE 6

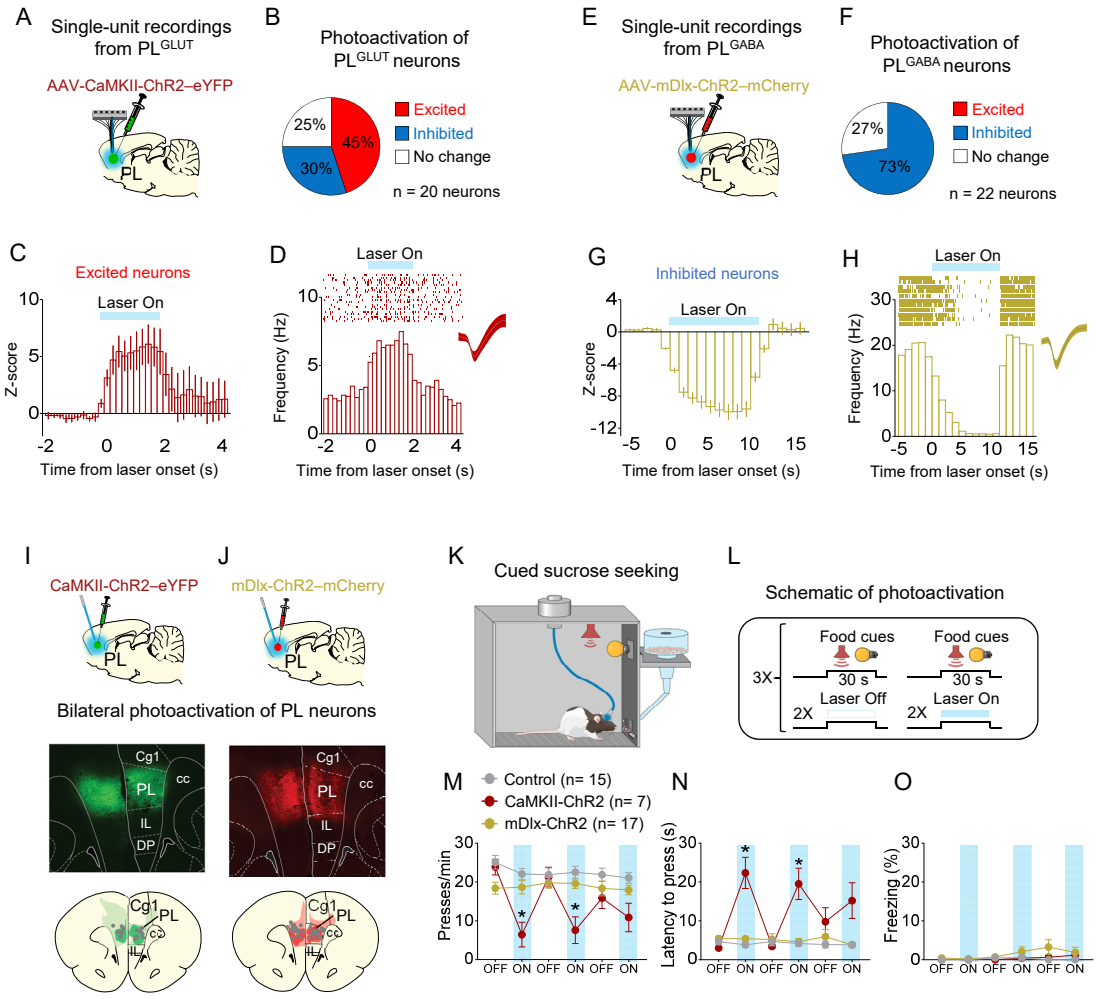

Figure 6. Photoactivation of PL^{GLUT}, but not PL^{GABA}, neurons suppresses reward seeking in a neutral context. (A) Schematic of viral infusion and recordings in PL. **(B)** Changes in PL firing rate with illumination of PL^{GLUT} neurons in rats expressing AAV-CaMKII-ChR2-eYFP in PL (n= 20 neurons). **(C)** Average PSTH of PL neurons that were excited during laser illumination of PL^{GLUT} neurons. **(D)** Raster plot and peri-stimulus time histogram (PSTH) of representative PL neuron showing excitatory responses to illumination in rats expressing AAV-CaMKII-ChR2-eYFP in PL. **(E)** Schematic of viral infusion and recordings in PL. **(F)** Changes in PL firing rate with illumination of PL^{GABA} neurons in rats expressing AAV-mDlx-ChR2-mCherry in PL (n= 22 neurons). **(G)** Average PSTH of PL neurons that were inhibited during laser illumination of PL^{GABA} neurons. **(H)** Raster plot and PSTH of representative PL neuron showing inhibitory responses to illumination in rats expressing AAV-mDlx-ChR2-mCherry in PL. **(I-J)** Representative micrograph showing the expression of (I) CaMKII-ChR2-eYFP or (J) mDlx-ChR2-mChery in PL and schematic of optical fiber location (gray dots) in the same region (compressed across different antero-posterior levels of PL). Green or red areas represent the minimum (dark) and the maximum (light) viral expression into the PL. **(K-L)** Schematic and timeline of PL photostimulation during the cued-sucrose seeking test in a neutral context. **(M-N)** Optogenetic activation of PL^{GLUT} neurons (CaMKII-ChR2, dark red circles, n= 7), but not PL^{GABA} neurons (mDlx-ChR2, gold circles, n= 17), reduced the (M) frequency of bar presses ($F_{(10, 180)} = 7.009$, $p<0.0001$, CaMKII-ChR2 OFF vs ON Tukey post hoc, $p < 0.0001$) and increased (N) the latency for the first press ($F_{(10, 180)} = 9.931$, $p < 0.0001$, CaMKII-ChR2 OFF vs ON Tukey post hoc, $p < 0.0001$) when compared to the control group (eYFP-control virus, gray circles, n = 15). **(O)** Optogenetic activation of PL neurons did not alter freezing behavior ($F_{(10, 180)} = 1.124$, $p = 0.3463$). Blue shaded area represents laser-on trials (PL^{GLUT}: 5 Hz, PL^{GABA}: 20 Hz; 5ms pulse width,7-10 mW, 30 s duration). Data shown as mean ± SEM. Each circle represents the average of two consecutive trials. Two-way repeated-measures ANOVA followed by Bonferroni post hoc test. All * p's < 0.05. All statistical analysis details are presented in table S1.

FIGURE 7

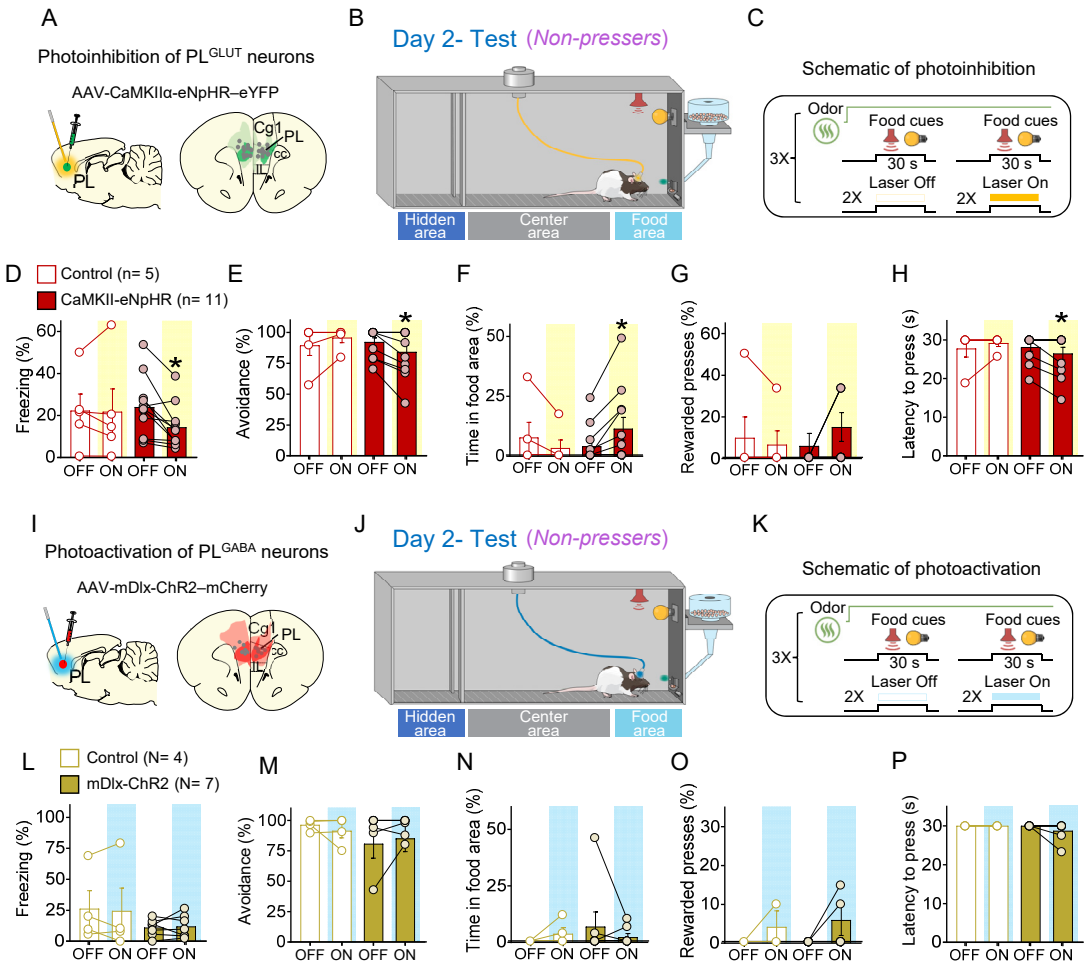

Figure 7. Photoinhibition of PL^{GLUT} neurons during conflict reduces freezing and increases food approaching in *Non-Pressers*. **(A)** Schematic of AAV-CaMKII-eNpHR–eYFP virus infusion in PL and location of optical fibers (gray dots) in the same region (compressed across different antero-posterior levels of PL). Green areas represent the minimum (dark) and the maximum (light) viral expression into the PL. **(B-C)** Schematic and timeline of the approach-avoidance conflict test during optogenetic inactivation of PL^{GLUT} neurons. **(D-H)** Photoinhibition of PL^{GLUT} neurons (CaMKII-eNpHR, red bars, n = 11) during the conflict test reduced the percentage of time rats spent (D) freezing (Wilcoxon test, W = -64, laser OFF vs. laser ON, p = 0.0020) and (E) avoiding the odor area (Wilcoxon test, W = -21, laser OFF vs. laser ON, p = 0.031) , and increased the percentage of time rats spent in the (F) food area (Wilcoxon test, W = -31, laser OFF vs. laser ON, p = 0.031) during the conflict test without altering (G) the number of lever presses (Wilcoxon test, W = 6, laser OFF vs. laser ON, p = 0.250) and (H) the latency to press (Wilcoxon test, W = -10, laser OFF vs. laser ON, p = 0.125), when compared to controls (eYFP-control virus, white bars, n= 5, Wilcoxon test, Freezing: W = 3, p = 0.812, avoidance: W = 3, p = 0.500, food area: W = 3, p = 0.500, lever presses: W = -1, p = 0.999, latency to press: W = 1, p = 0.999). **(I)** Schematic of AAV-mDlx-ChR2–mCherry virus infusion in PL and location of optical fibers (gray dots) in the same region (compressed across different antero-posterior levels of PL). Red areas represent the minimum (dark) and the maximum (light) viral expression into the PL **(J-K)** Schematic and timeline of the approach-avoidance conflict test during optogenetic activation of PL^{GABA} neurons. **(L-P)** Photoactivation of PL^{GABA} neurons during the conflict test did not alter rats' behavior (mDlx-ChR2, gold bars, n= 7, Wilcoxon test, Freezing: W = 18, p = 0.156, avoidance: W = 4, p = 0.500, food area: W = -2, p = 0.750, lever presses: W = 3, p = 0.500, latency to press: W = -3, p = 0.500), when compared to controls (eYFP-control virus, white bars, n = 4, Wilcoxon test, Freezing: W = -2, p = 0.875, avoidance: W = 0, p = 0.999, food area: W = 3, p = 0.500, lever presses: W = 1, p = 0.500, latency to press: all animals reached maximum latency). PL neurons were illuminated from cue onset until the animals pressed the bar or from cue onset until the end of the 30s cues if the animals didn't press the bar (PL^{GLUT}: 5 Hz, PL^{GABA}: 20 Hz; 5ms pulse width,7-10 mW). Data shown as mean ± SEM. Each bar represents the average of six trials alternated in blocks of 2. Note that the number of data points may appear fewer than the number of rats per group because multiple animals showed the same values. Two-way ANOVA repeated measures followed by Bonferroni post hoc test. All * p's < 0.05. All statistical analysis details are presented in table S1. See also Supplementary Fig 8.

FIGURE 8

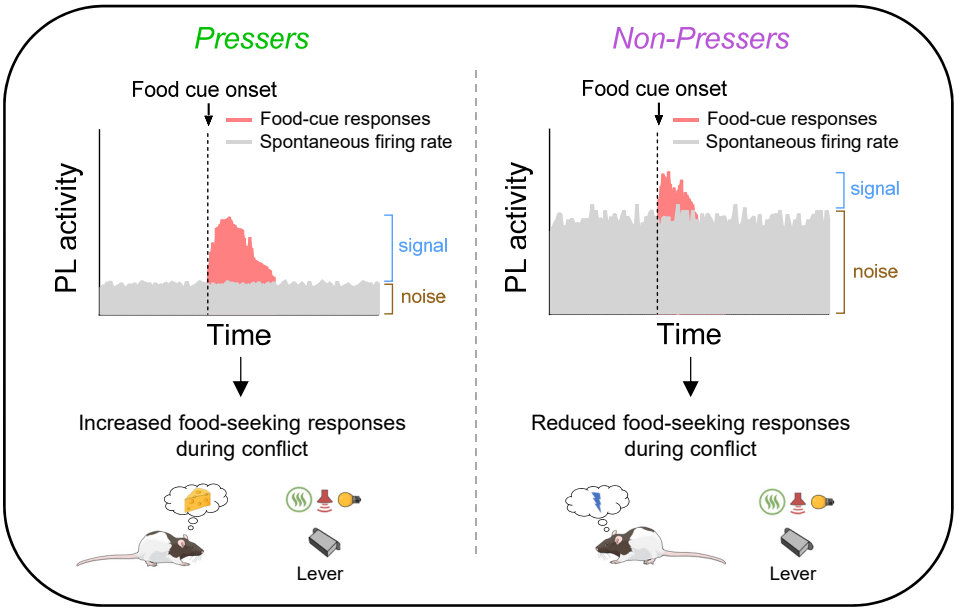

Figure 8. Schematic showing differences in food-cue responses and spontaneous firing rate of PL neurons in *Pressers* and *Non-Pressers.* Left, *Pressers* showed reduced spontaneous firing rate and increased food-cue responses in PL neurons during the conflict test, which resulted in higher signal-to-noise ratio and increased food-seeking responses. Right, *Non-Pressers* showed increased spontaneous firing rate and reduced food-cue responses in PL neurons during the conflict test, which resulted in lower signal-to-noise ratio and reduced food-seeking responses.